Lithos 372–373 (2020) 105681

Contents lists available at ScienceDirect

Lithos

journal homepage: www.elsevier.com/locate/lithos

Mineralogy of the HSE in the subcontinental lithospheric mantle — An interpretive review

José M. González-Jiménez [a,*], Santiago Tassara [b], Erwin Schettino [c], Josep Roqué-Rosell [d], Julia Farré-de-Pablo [d], J. Edward Saunders [e], Artur P. Deditius [f], Vanessa Colás [g], Juan J. Rovira-Medina [a], María Guadalupe Dávalos [h], Manuel Schilling [i], Abigail Jimenez-Franco [d,j], Claudio Marchesi [a,c], Fernando Nieto [a,c], Joaquín A. Proenza [d], Fernando Gervilla [a,c]

[a] Departamento de Mineralogía y Petrología, Facultad de Ciencias, Universidad de Granada, Avda. Fuentenueva s/n, 18002 Granada, Spain
[b] Department of Earth and Planetary Sciences, Yale University, PO BOX 208109, New Haven, CT 06520-8109, U.S.A
[c] Instituto Andaluz de Ciencias de la Tierra (IACT), CSIC-UGR, Avda. de las Palmeras 4, 18100, Armilla, Granada, Spain
[d] Departament de Mineralogia, Petrologia i Geologia Aplicada, Facultat de Ciències de la Terra, Universitat de Barcelona, 08028 Barcelona, Spain
[e] Division of Earth Sciences, School of Environmental and Rural Science, University of New England, Armidale, NSW 2351, Australia
[f] Discipline of Chemistry and Physics, College of Science, Health, Education and Environment (CSHEE), Murdoch University, Murdoch 6150, WA, Australia
[g] Instituto de Geología, Universidad Nacional Autónoma de México, Ciudad Universitaria, 04510 Ciudad de México, Mexico
[h] Facultad de Ciencias, Universidad Nacional Autónoma de México, Ciudad Universitaria, 04510 Ciudad de México, Mexico
[i] Instituto de Ciencias de la Tierra, Universidad Austral de Chile, Valdivia 5090000, Chile
[j] Posgrado en Ciencias de la Tierra, Universidad Nacional Autónoma de México, Ciudad Universitaria, Delegación Coyoacán, 04510 Cd. de México, Mexico

ARTICLE INFO

Article history:
Received 30 January 2020
Received in revised form 29 June 2020
Accepted 5 July 2020
Available online 14 July 2020

Keywords:
Sulfides
Platinum-group minerals
Nanoparticles
Subcontinental lithospheric mantle
Partial melting
Metasomatism

ABSTRACT

The highly siderophile elements (HSE: Os, Ir, Ru, Rh, Pt, Pd, Re, Au) exist in solid solution in accessory base-metal sulfides (BMS) as well as nano-to-micron scale minerals in rocks of the subcontinental lithospheric mantle (SCLM). The latter include platinum-group minerals (PGM) and gold minerals, which may vary widely in morphology, composition and distribution. The PGM form isolated grains often associated with larger BMS hosted in residual olivine, located at interstices in between peridotite-forming minerals or more commonly in association with metasomatic minerals (pyroxenes, carbonates, phosphates) and silicate glasses in some peridotite xenoliths. The PGM found inside residual olivine are mainly Os-, Ir- and Ru-rich sulfides and alloys. In contrast, those associated with metasomatic minerals or silicate glasses of peridotite xenoliths consist of Pt, Pd, and Rh bonded with semimetals like As, Te, Bi, and Sn. Nanoscale observations on natural samples along with the results of recent experiments indicate that nucleation of PGM is mainly related with the uptake of HSE by nanoparticles, nanominerals or nanomelts at high temperature (> 900 °C) in both silicate and/or sulfide melts, regardless of the residual or metasomatic origin of their host minerals. A similar interpretation can be assumed for gold minerals. Our observations highlight that nanoscale processes play an important role on the ore-forming potential of primitive mantle-derived magmas parental to magmatic-hydrothermal deposits enriched in noble metals. The metal inventory in these magmas could be related with the physical incorporation of HSE-bearing nanoparticles or nanomelts during processes of partial melting of mantle peridotite and melt migration from the mantle to overlying continental crust.

1. Introduction

The highly siderophile elements (HSE), also known as the noble or precious metals, include the six platinum-group elements (PGE: Os, Ir, Ru, Rh, Pt, Pd) along with Re and Au. Experimental studies have shown that these transition metals have a strong affinity for iron (siderophile affinity) as reflected in their high (10^5–10^8) metal/silicate melt partition coefficients over a large range of temperature and pressure conditions (e.g., Brenan et al., 2016; Mann et al., 2012). However, observations on natural mantle rocks show that the inventory of the HSE in the Earth's upper mantle is mostly stored in accessory (< 1% modal) base-metal sulfides (BMS) of the Ni-Fe-Cu system rather than alloys (Luguet and Reisberg, 2016), revealing that they are both siderophile and chalcophile elements in nature. This is because most terrestrial magmatic systems are relatively oxidized (above the

* Corresponding author.
E-mail address: jmgonzj@ugr.es (J.M. González-Jiménez).

https://doi.org/10.1016/j.lithos.2020.105681
0024-4937/

iron-wustite buffer), such that native Fe is not stable. Consequently, the HSE also display very high partition coefficients for sulfide in magmatic systems (e.g., Li and Audétat, 2013; Mungall and Brenan, 2014).

In the Earth's upper mantle, the HSE may also form their own minerals essentially constituted by PGE, which are known as as platinum-group minerals (PGM). The latter may include alloys, sulfides, arsenides, sulfarsenides, tellurides, bismuthides, or stannides (O'Driscoll and González-Jiménez, 2016 and references therein). Most of our knowledge of the variety and distribution of the PGM in the upper mantle comes from the study of chromite-rich rocks (i.e., chromitites) hosted in mantle peridotites from ophiolite complexes. In this setting, the PGM form by both magmatic (i.e., primary) and post-magmatic (i.e., secondary related to serpentinization, hydrothermal alteration, metamorphism and weathering) processes (O'Driscoll and González-Jiménez, 2016).

In the field of SCLM research, the mineralogy of the HSE is only recently beginning to receive the attention it deserves, very likely reflecting the fact that most previous studies have focused their effort on the analysis of HSE apparently dissolved in solid solution in the BMS (e.g., Luguet and Reisberg, 2016). In many studies, the inspection of the time-resolved spectra collected during LA-ICP-MS analysis revealed unexpectedly high concentration of HSE in some mantle BMS, which might correspond to tiny minerals and particles of HSE (e.g., Alard et al., 2011; Hughes et al., 2017; Wang et al., 2009). A more accurate picture of the mineralogy of HSE in the SCLM is available from the study of peridotite massifs cropping out in the French Pyrenees (e.g., Ferraris and Lorand, 2015; Lorand et al., 2010; Luguet et al., 2007) where the mineralogy of the HSE has comparatively better-studied using a wider range of analytical techniques than in other peridotite samples from the SCLM such as ultramafic xenoliths (with some notable exceptions, as outlined in Section 2). Of particular importance are the recent studies showing the existence of nano-sized PGM and gold particles in peridotite xenoliths from both cratonic (Wainwright et al., 2016) and off-craton regions (González-Jiménez et al., 2019; Tassara et al., 2017). These new advances suggest a critical role of nanoscale processes in controlling HSE fractionation, transport and concentration in the SCLM.

This paper provides a state-of-the-art of the mineralogy of the HSE, at the nano- and micron-scales, in different rock suites of the SCLM. Our main purpose is to foster the debate about the origin of these minerals in rocks from the SCLM and its potential implications for our understanding of HSE geochemical behavior in the upper mantle. To achieve this goal, we focus on ultramafic xenoliths and mineral xenocrysts hosted in on- and off-craton volcanic rocks as well as on exhumed fragments of the SCLM (i.e., orogenic peridotites) ranging in age from the Archean to the Quaternary (Fig. 1). Furthermore, in order to provide an up-to-date picture of the origin of HSE-bearing minerals in the SCLM, we also compare the different genetic models proposed in the literature, taking into account the microstructural location of the minerals. Our interpretive review is based on the integration of information acquired from the pre-existing literature with our novel research on peridotite xenoliths sampling regions of the SCLM underlying continental crust with a strong metal endowment (Section 3 and Appendix 1). Our sample selection aims to explore how PGM-forming mechanism impact in the generation of metal-rich magmas in metallogenic provinces. We strongly emphasize on the new results provided by using a combination of focused ion beam and high-resolution transmission electron microscopy (FIB/HRTEM). The focused ion beam (FIB) tool has been successfully used to prepare site-specific electron transparent thin foils from minerals, which enables high-resolution (cross-section) imaging by high-resolution transmission electron microscopy (HRTEM). The combination of FIB and scanning-electron microscopy (SEM) methods applied to minerals represents an in-situ approach for sample characterization and thus provides relevant crystal–chemical data that can be placed into the geological context (Ciobanu et al., 2011; Junge et al., 2015; Lee, 2010; Wirth, 2004, 2009; Wirth et al., 2013).

2. Previous reports of HSE-bearing nano and micron-sized minerals in the subcontinental lithospheric mantle

2.1. Off-craton peridotite xenoliths

The first ever PGM reported in rocks from the SCLM were two grains (~500 nm) of cooperite (PtS) and paolovite (Pd_2Sn), which were found in partly desulfurized pentlandite blebs hosted in olivine and metasomatic pyroxene, respectively, within lherzolite xenoliths from the SCLM beneath Mount Porndon in southeastern Australia (Fig. 1; Keays et al., 1981). According to Keays et al. (1981) the PGM exsolved at low temperatures (<300 °C) from pentlandite formed by the breakdown of former Fe—Ni monosulfide solid solution (MSS).

Several decades later, Wang et al. (2009) discovered Pt-rich micronuggets in Fe-rich MSS in non-cratonic peridotite nodules from the Penghu Islands, Taiwan (Fig. 1). The nuggets were identified as sharp spikes in the Pt signal of the time-resolved LA-ICP-MS spectra, although they could not fully confirm the nature of PGM by other analytical techniques.

Alard et al. (2011) and Delpech et al. (2012) also identified several grains of Pt-Te-Bi and Pt-Pd-As (including sperrylite $PtAs_2$) in spinel-peridotite xenoliths from Montferrier (Languedoc, France, Fig. 1) and in dunite xenoliths from the Kerguelen Archipelago (France, Fig. 1). These PGM were associated with pentlandite-chalcopyrite (± cubanite) blebs coexisting with interstitial metasomatic carbonates, and were detected by SEM-BSE imaging on polished thin sections and during in situ LA-ICP-MS analysis of the same samples. Alard et al. (2011) and Delpech et al. (2012) suggested that Pt-bismuthotellurides formed by fractional crystallization of a Cu-Ni-rich sulfide melt whereas Pt-Pd-rich arsenides crystallized at temperatures below or near 900 °C (i.e., below the solidus of the sulfide) by the reaction of sulfide-hosted Pt-bismuthotellurides with volatile-rich fluids that refertilized the SCLM.

Other PGM found in off-craton peridotite xenoliths include Pt-alloys reported by O'Driscoll and González-Jiménez (2016) associated with Fe-rich MSS located at olivine interstices in lherzolite xenoliths from the Calatrava Volcanic Field, central Spain (Fig. 1). González-Jiménez et al. (2019) also reported nanometer-sized (< 100 nm) grains of hongshiite (PtCu) and tulameenite (Pt_2CuFe) hosted in pentlandite embedded in metasomatic silicate glasses from mantle lherzolite xenoliths from Cerro Redondo and Gobernador Gregores in southern Patagonia. González-Jiménez and co-workers (2019) suggested that these Pt-rich nanoalloys as well as other nanometer-sized Pt-rich arsenides found in these interstitial glasses could have been segregated directly from the infiltrating alkaline basaltic melt prior to sulfide saturation in the silicate melt, or from droplets of immiscible sulfide melt once sulfide saturation was achieved. Tassara et al. (2017) proposed a similar interpretation to explain the origin of gold particles (< 2 μm) embedded in interstitial metasomatic silicate glass veins and associated BMS (millerite and chalcopyrite) also present within a lherzolite xenolith from Cerro Redondo. Finally, Mundl et al. (2015) identified a micron-sized grain of laurite (RuS_2) at the boundary between metasomatic clinopyroxene and orthopyroxene in a harzburgitic xenolith from Puesto Díaz in the North Patagonian Massif. These authors suggested that laurite could have precipitated from a sulfur-undersaturated metasomatic silicate melt percolating by porous flow through the SCLM, although they did not explain the specific mechanism accounting for laurite crystallization.

2.2. Peridotite xenoliths and olivine xenocrysts sampling on-craton SCLM

Several PGM grains have been detected within mantle xenolith samples of the SCLM in cratonic regions, including (Fig. 1):

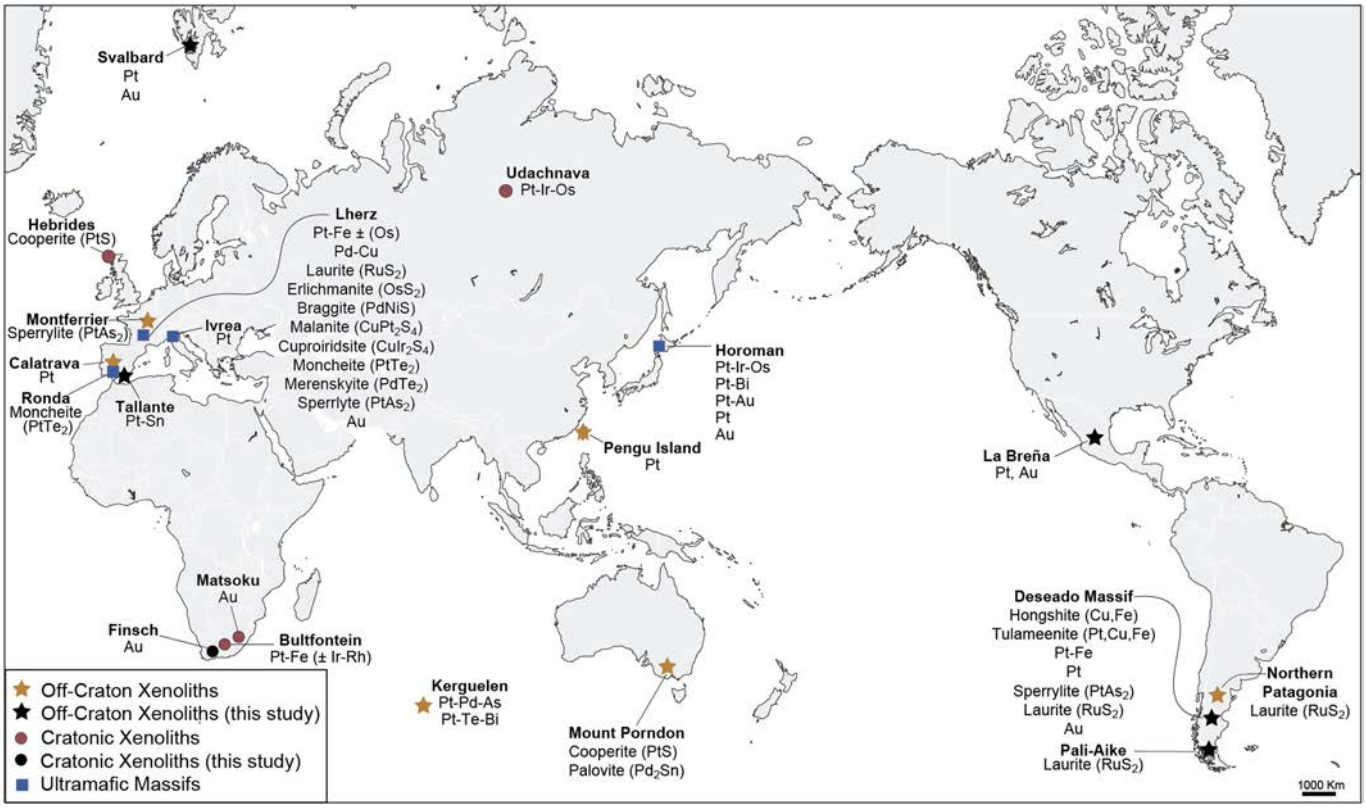

Fig. 1. Global map showing the distribution of localities sampling rocks of the Subcontinental Lithospheric Mantle (SCLM) where discrete minerals of the highly siderophile elements (HSE) have been reported. This map also includes the new discoveries of HSE minerals reported in this study. References for the different localities are in the main text.

(1) micron-sized Pt-Ir-Os in MSS grains enclosed in olivine crystals from mantle peridotites trapped by the Udachnaya kimberlite (Siberian craton; Griffin et al., 2002). These Pt-Ir-Os alloys were identified by Griffin et al. (2002) by inspecting the time-resolved signals collected during LA-ICP-MS. These authors suggested a residual origin for these alloys as a result of small degrees of partial melting of a pre-existing BMS in a mantle region under sulfur undersaturated conditions.

(2) Pt-rich sulfide grains (possibly cooperite, PtS) in lherzolite xenoliths collected from the cratonic Hebridean Terrane (localities of Loch Roag and Rinibar) in northwest Scotland (Hughes et al., 2016). These cooperite grains were observed within the chalcopyrite portion of a composite sulfide (pyrrhotite-pentlandite-chalcopyrite)-carbonate bleb, along the margin with pyrrhotite. The composite sulfide assemblage was interstitially located between primary silicates of the peridotitic matrix, and interpreted to have formed upon cooling of a sulfide liquid.

(3) micron-sized Pt—Fe (±Ir-Rh) alloys included in two pentlandite grains (forming composite aggregates with pyrrhotite) within a single cratonic harzburgite sampled by the Bultfontein kimberlite (Kaapvaal craton, South Africa; Wainwright et al., 2016). One PGM-pentlandite grain (i.e., blocky pentlandite) was observed partially included in a serpentinised olivine such that one face of the BMS was in contact within the interstitial medium, whereas the second pentlnadite grain was enclosed (along with phlogopite) within metasomatic clinopyroxene. The FIB-TEM characterization on thin foils indicates that PGM (<1 μm long and ~ 75 nm width) in olivine-hosted blocky pentlandite were misoriented relative to the sulfide matrix. On the other hand, PGM (1–5 μm long and < 500 nm width) found in the clinopyroxene-hosted pentlandite form oriented lamellae within the sulfide matrix. According to Wainwright et al. (2016) the two distinct BMS, as well as their Pt–Fe-alloy inclusions, represent different stages of a single sequence of fractional crystallization and subsolidus re-equilibration of a Ni-rich sulfide matte. In this case, the blocky pentlandite and Pt–Fe-alloys crystallized at higher temperature (i.e., 760 °C) relative to the pentlandite-pyrrhotite exsolution and their numerous texturally aligned Pt–Fe-alloys (<610 °C).

2.3. Exhumed ultramafic massifs

HSE-bearing minerals reported in peridotite samples from the SCLM exhumed in orogenic belts (i.e., orogenic peridotite massifs) include: (1) an euhedral (cubic) inclusion of Pt-Fe-Ni (87.0 wt% Pt, 11.2 wt% Fe and 2.22 wt% Ni) about 6 × 5 μm in size within a pentlandite grain interstitial to primary silicates on a lherzolite sample from Balmuccia (Ivrea Complex, northern Italy) (Garuti et al., 1984), (2) a grain of moncheite ($PtTe_2$) < 2 μm wide within olivine-hosted pentlandite from a spinel-bearing clinopyroxenite dyke from the Ronda massif in southern Spain (Fig. 1; Gutiérrez-Narbona, 1999), and (3) several (>100 grains) PGM and gold minerals from the Lherz massif and its cluster of peridotite outcrops (Ariége, Freychinède, Fontête Rouge) in the French Pyrenees (Fig. 1; Luguet et al., 2007; Lorand et al., 2010; König et al., 2015). The suite of HSE-bearing minerals identified in the French ultramafic massifs include micron to submicron grains of Ru—Os sulfides [members of the laurite (RuS_2)– erlichmanite (OsS_2) solid solution series], Pt-Ir-Cu ± Rh sulfides [members of the malanite ($CuPt_2S_4$) – cuproiridsite ($CuIr_2S_4$) solid solution series, braggite (PdNiS)], Pt-Pd-Te-Bi minerals [moncheite ($PtTe_2$) – merenskyite ($PdTe_2$)], sperrlyite ($PtAs_2$), as well as Pt-Ir ± (Os) alloys, and an unidentified Pd—Cu mineral. All these PGM were systematically associated with BMS, and were detected on polished thin sections and during in situ LA-ICP-MS analysis of BMS

(Lorand et al., 2010), as well as by X-ray micro-CT scanning of the peridotite samples (König et al., 2015). Most of the BMS were located along mineral grain boundaires of the peridotite matrix, or enclosed in olivine crystals, except one grain of pure platinum included within a Cr-spinel grain. Laurite-erlichmanite and Pt–Ir–Os alloys were interpreted as refractory minerals formed after partial melting (20–30%) of a former MSS, very likely prior to the complete consumption of the MSS (König et al., 2015; Luguet et al., 2007). According to Lorand et al. (2010) such formation of the PGM as residual phases might be attributed to a series of partial melting events in the (~2 Ga) SCLM, which removed the BMS and left refractory PGM as stable minerals under S-undersaturated conditions. In contrast, the minerals of the malanite-cuproiridiste solid solution series, sperrylite and the Pt-Pd-Te-Bi system were interpreted to have formed via subsolidus re-equilibration of S- and Cu-rich, volatile-rich, small melt fractions that metasomatized the Lherz SCLM.

Lorand et al. (2010) also noted that the peridotite samples hosting PGM in Lherz contain micron-sized grains of native gold, which were observed filling fractures or close to the altered contact between chalcopyrite and pentlandite. A few years later, Ferraris and Lorand (2015) identified micrometric inclusions of novodneprite ($AuPb_3$), anyuiite [$Au(Pb,Sb)_2$] and nanometric clusters of gold in olivine grains of these peridotites using HRTEM and electron energy loss spectroscopy (EELS). According to these authors, novodneprite and anyuiite formed during subsolidus recrystallization of the Pyrenean lherzolites following the growth of secondary olivine that trapped inter-granular components. Ductile deformation likely triggered the formation of dislocations within the olivine grains and enhanced the circulation of metasomatic Au-enriched fluids.

The coexistence of PGM and gold was also reported in a spinel lherzolite from the Horoman peridotite complex (Japan) (Fig. 1). In this sample from the SCLM, Kogiso et al. (2008) identified nine grains of PGM alloys (~1 to 10 μm), including Os—Ir, Os–Ir–Pt, Pt—Bi Pt—Au, Pt, and Au, using microbeam synchrotron radiation X-ray fluorescence analysis. All these grains were located near, or within, pentlandite grains interstitially distributed among primary olivine and pyroxene. However, no explanation for the origin of these PGM and gold minerals was provided.

3. New discoveries of PGM and gold minerals, and nanoparticles in SCLM xenoliths

In this study, we also report new nano- and micron-sized minerals and particles of the HSE in different microtextural locations within SCLM xenoliths (lherzolites and harzburgites) from on- and off-craton regions. In-situ textural data, instead locality of the rock, are used as platform criteria to describe and compare our data with previously published work. It makes it easier to critically evaluate the different proposed models that attempt to explain the origin of the platinum-group mineral in the SCLM. Thus, new descriptions of PGMs in mantle xenolith come from South America (Deseado Massif and Pali-Aike in the Argentinian Patagonia), North America (La Breña in the Durango Volcanic Field in Central Mexico), Southern Europe (Tallante in the Cabo de Gata-Cartagena Volcanic Belt in southern Spain), northwest Europe (Spitsbergen in Svalbard archipelago in northern Norway) and South Africa (Finsch mine in South Africa and Matsoku kimberlites in Northern Lesotho). Information about the provenance and petrology of each sample, and background information regarding the analytical procedures used to characterize their HSE-bearing minerals in all samples, are provided in Appendix 1 and 2, respectively.

3.1. Pt—Fe alloys and laurite in base-metal sulfide blebs enclosed in residual olivine

We found PGE-rich nanoparticles enclosed within a composite sulfide aggregate consisting of monoclinic Ni-rich pyrrhotite and pentlandite, which is hosted in a residual olivine grain from a peridotite xenolith from Tres Lagos (southern Patagonia; sample TL-2-1) (Fig. 2A-G; Appendix 3–5). The obtained field emission scanning electron microscopy (FESEM) and energy dispersive spectra (EDS) (Appendix 4) revealed two types of nanoparticles consisting of Pt—Fe and Ru-Os-S. However, many of these minerals were too small for reliable identification and/or quantitative analyses.

The FIB thin-foil cut through the contact between the pyrrhotite and pentlandite crystals of this composite inclusion in olivine intersected three of these PGE-rich nanoparticles (Fig. 3). Two of the nanoparticles (A and C in Fig. 4) are enclosed in pyrrhotite whereas the third nanoparticle (B in Fig. 4) was found in pentlandite (Fig. 4A-C). The longest dimension of the nanoparticles is ~500 nm. The high-angle annular dark-field (HAADF) images obtained by means of HRTEM for all these nanoparticles show that they are homogenous crystals containing rounded inclusions (<30 nm) of a Fe—O compound (Fig. 4A-C). The corresponding fast Fourier transform (FFT) patterns allow us to identify these crystalline nanoparticles as laurites (RuS_2) embedded in a distinctly oriented matrix of a defective monoclinic pyrrhotite and pentlandite (Fig. 5A–C; Appendix 5). Laurite grains are characterized internally by a compositional core-to-rim Os enrichment (Fig. 4A–C; i.e., normal zoning as defined by González-Jiménez et al. (2009) for members of the laurite [RuS_2]-erlichmanite [OsS_2] solid solution series). The nanostructural analysis of one of the rounded FeO compounds (particle enclosed in the dotted rectangles B3 shown in Fig. 5) reveals a well-crystallized magnetite (with the corresponding d-spacing (400) at 2.09 Å) with no crystallographic continuity relative to its laurite host (d-spacing (111) at 3.2 Å) (Appendix 5). In addition, the analysis of the HRTEM images and FFT indicates the presence of irregular contacts and crystal misorientations between pyrrhotite and pentlandite even at the nanoscale (Figs. 3 and 5).

3.2. Native Pt, Pt-rich tellurides and stannides associated with base-metal sulfides in metasomatic pyroxenes

Base-metal sulfides hosted in metasomatic clinopyroxenes from Tres Lagos (southern Patagonia; sample PM-11) contain submicron (~500 nm to ~2 μm) crystals of native platinum (Fig. 6A, A1 and A2; Appendix 3–4). Noteworthy, these nano-PGM are located at the margin of the chalcopyrite portion of the sulfide globule, which consists of a polyphase assemblage made up of Ni-rich pyrrhotite, pentlandite and chalcopyrite.

Two grains of a Pt—Te mineral (possibly moncheite, $PtTe_2$) of <2 μm in diameter were identified in a xenolith collected from southern Patagonia at the eruptive center of Cerro Redondo (Fig. 6B; sample CR-01). Both grains were associated with pentlandite and located in the core of the sulfide or along the contact with chalcopyrite.

Metasomatic clinopyroxene and orthopyroxene from mantle xenoliths of Tallante (eastern Betics, southeast Spain) contain pentlandite blebs hosting nano-to-micro (<1.5 μm in diameter) particles of a Pt—Sn mineral (Fig. 6C-E; Appendix 3–5). These grains exhibit euhedral morphologies and are commonly located at the margin of pentlandite grains in contact with a silicate melt inclusion (Fig. 6C) or chalcopyrite (Fig. 6E), or the Pt—Sn particles may be entirely enclosed within pentlandite (Fig. 6D). A FIB section of the Pt—Sn particle shown in Fig. 6E-1 reveals euhedral shape with sharp contacts with pentlandite, magnetite and chalcopyrite (Fig. 7-9). The magnetite is located between Pt—Sn and chalcopyrite. The TEM-EDS elemental mapping of the Pt-Cu-Sn particle shows homogeneous distribution of Pt, Cu, Sn and Pd (Fig. 8). The FFT analysis of the HRTEM images of the associated minerals revealed that pentlandite, magnetite, and tatyanaite [ideally ($Pt_9Cu_3Sn_4$] are single crystals. Tatyanaite was identified based on the corresponding d-spacing (100) at 2.30 Å. There is lack of crystallographic continuity between tatyanaite and host pentlandite and associated magnetite (Fig. 9; Appendix 5).

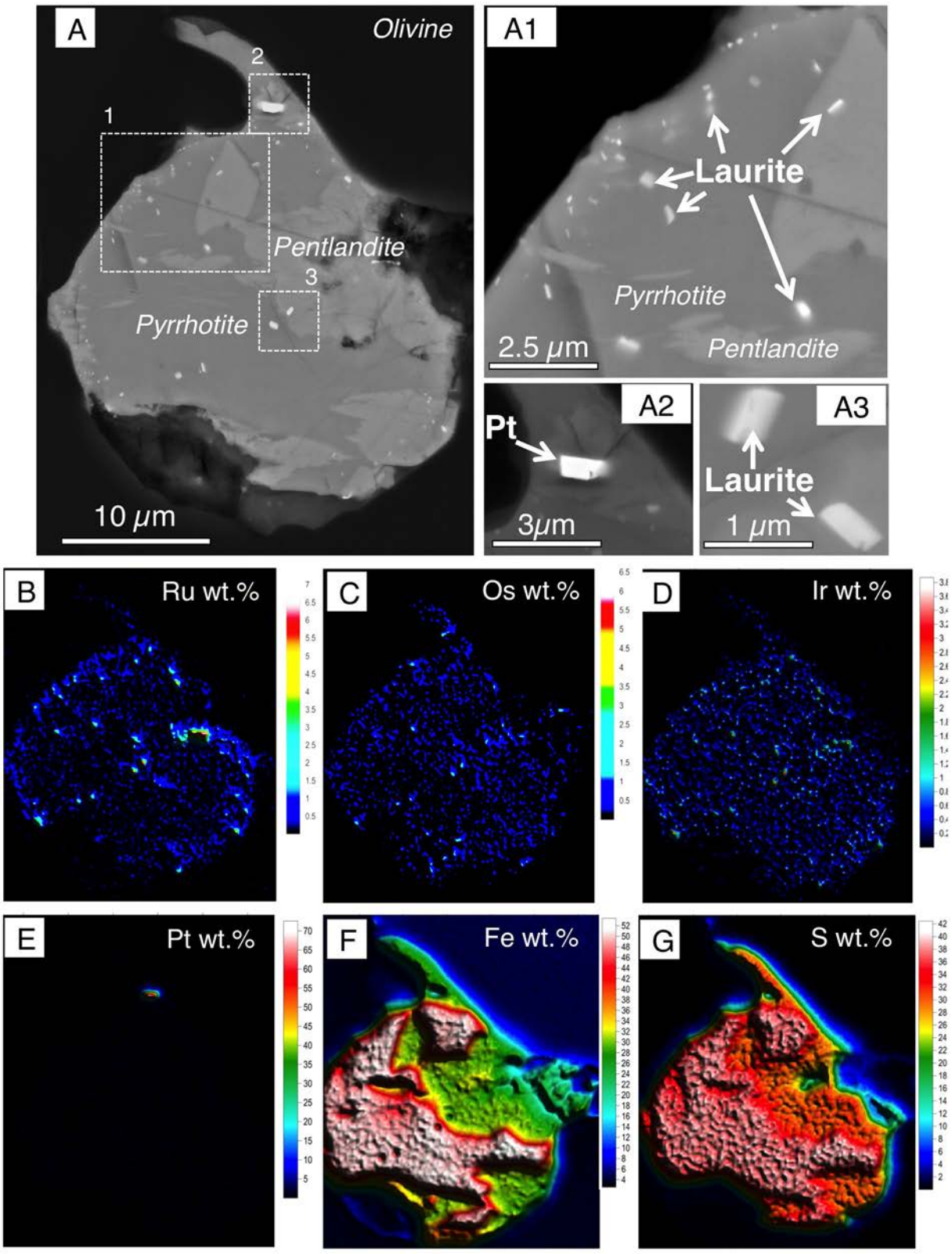

Fig. 2. (A) Backscattered images of the PGM-bearing base-metal sulfide bleb hosted in a residual olivine grain from a peridotite xenolith from Tres Lagos in southern Patagonia (sample TL-2-1). (B-G) Quantitative, wavelength-dispersive spectrometry (WDS) X-ray elemental maps of sulfide bleb. Note the heterogeneous distribution of Ru and Pt indicating the presence of nanoparticles.

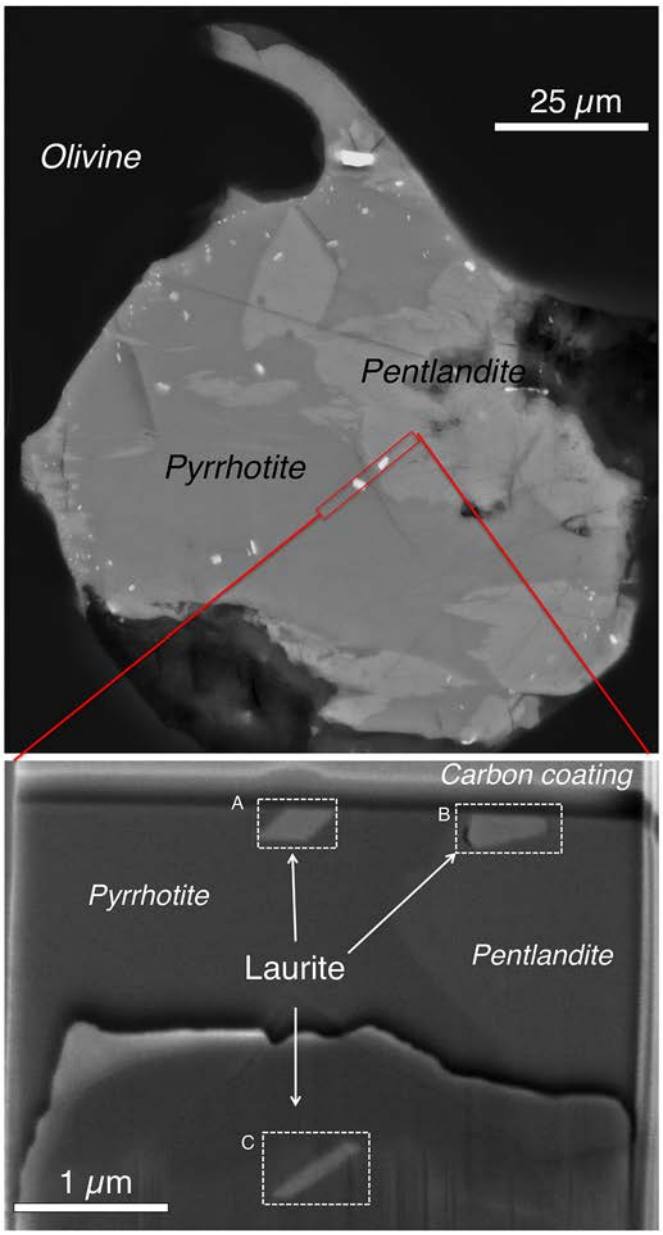

Fig. 3. Back-scattered images of thin-foil sampled from the Tres Lagos PGM-bearing base-metal sulfide blebs shown in Fig. 2. The three nano-PGM identified as laurite that were intersected during sample preparation are enclosed in the rectangles and named as shown in Figs. 4 and 5.

3.3. Nanoparticles of Pt-Pd ± S ± Te ± as and laurite in silicate glasses and associated base-metal sulfides

Pt-rich (<1 μm) particles occur as pentlandite-hosted inclusions embedded within interstitial silicate glass in xenoliths from Gobernador Gregores in Patagonia (Fig. 10A; replicates of the sample GG-14 analyzed by González-Jiménez et al., 2019) as well as in xenoliths from La Breña in Central Mexico (Fig. 10B-C; samples LB-1 and LB-3). Some of these pentlandite grains are frequently altered to oxy-hydroxides.

Other pentlandite blebs entrained in the interstitial glass of xenoliths from southern Patagonia contain Pd-rich minerals, including: (1) Pd—S (possibly braggite, PdS) located at the contact between pyrrhotite and pentlandite from a xenolith in Gobernador Gregores (Fig. 10D; sample GG-01), and (2) Pd—Te (possibly merenskyite, $PdTe_2$) and Pt—As (possibly sperrylite $PtAs_2$) found at the grain boundaries between pentlandite and millerite in the xenoliths from Cerro Redondo (Fig. 10E-G; replicates of samples CR-08 studied by Tassara et al., 2017).

Two grains of a Ru—S mineral (possibly laurite, RuS_2) were observed within the interstitial glass in samples from southern Patagonia in the localities of Cerro Redondo (sample CR-08) and Pali-Aike (sample PA-LA7) (Fig. 10H-J).

3.4. Gold

We have also identified nanometer-sized particles of native gold in pentlandite grains hosted in metasomatic clinopyroxenes from the Tallante xenoliths in southern Spain (Fig. 11A-B and Appendix 6; samples TAL-110, TAL-129). Moreover, native gold was also observed within the chalcopyrite portion of composite pentlandite-chalcopyrite aggregates entrained in the interstitial glass of southern Patagonian xenoliths (Figs. 11C-D and 12; sample CR-08 studied by Tassara et al., 2017). Nanoparticles of gold, often coexisting with Pt, are also common in partly altered pentlandite droplets in the interstitial glass of mantle xenoliths from La Breña in Central Mexico (Fig. 11E-G; samples LB-1 and LB-3).

In addition, a re-examination of the time-resolved data acquired during LA-ICP-MS analysis of sulfides hosted in metasomatized spinel lherzolites from Svalbard (Saunders et al., 2015) and garnet lherzolites and harzburgites from the Kaapvaal Craton (Griffin et al., 2004) has revealed the presence of several micron-sized nuggets of gold in BMS (Appendix 6). These BMS consisting of MSS or pentlandite are also associated with metasomatic silicate glasses or pyroxene.

4. Discussion

4.1. The origin of nano-PGM associated with BMS included in residual olivine

The BMS grain from Tres Lagos shown in Figs. 2-5 exhibits a droplet-shaped suggesting its crystallization from a former immiscible sulfide melt droplet being mechanically trapped by growing olivine (e.g., Andersen et al., 1987; Szabó and Bodnar, 1995). This inclusion consists of Ni-rich pyrrhotite and pentlandite, indicating that even though the immiscible sulfide melts were segregated before or contemporaneously to olivine crystallization at >1000 °C (Tassara et al., 2018), the observed sulfide assemblage is not primary owing to the lower thermal stability of pentlandite (< 870 °C; Sugaki and Kitakaze, 1998; Kitakaze et al., 2016). The irregular contacts between pyrrhotite and pentlandite at the micron (Fig. 2) and nanoscale (Fig. 3), as well as the different orientation of their crystal lattice, may suggest the possible formation of pentlandite by a peritectic reaction of MSS crystallites (now represented by Ni-rich pyrrhotite) with a Ni-richer melt (e.g., Kitakaze et al., 2016; Sugaki and Kitakaze, 1998). However, the reconstructed composition of the original sulfide (Appendix 4) falls within the mixing line between the measured composition of pyrrhotite and pentlandite. This suggests that Ni was not added to the system as would be expected if a peritectic reaction formed pentlandite. Therefore, these micro- and nano-structural relationships simply reflect the low temperature exsolution of granular and flame-like pentlandite at <610 °C, from re-equilibrating MSS.

The residual nature of the host olivine links the origin of this BMS grain with partial melting events experienced by the host rock (Alard et al., 2002). Experimental (Bockrath et al., 2004a; Fonseca et al., 2012; Peregoedova et al., 2004) and empirical (Barnes et al., 2016; Luguet et al., 2007) results show that variable rates of partial melting of BMS under decreasing fS_2 at ≥1000 °C may result in the formation of Os, Ir, Ru and Pt enriched residual Fe-rich MSS with coexisting Ni-rich melts/solids (< 10% partial melting) or PGM (laurite, Os-Ir-Ru or Pt—Fe alloys; 10–20% partial melting). In this scenario, nano-sized laurite grains enclosed in both pyrrhotite and pentlandite (Figs. 2 and 3) may be interpreted as the result of high-temperature exsolution during

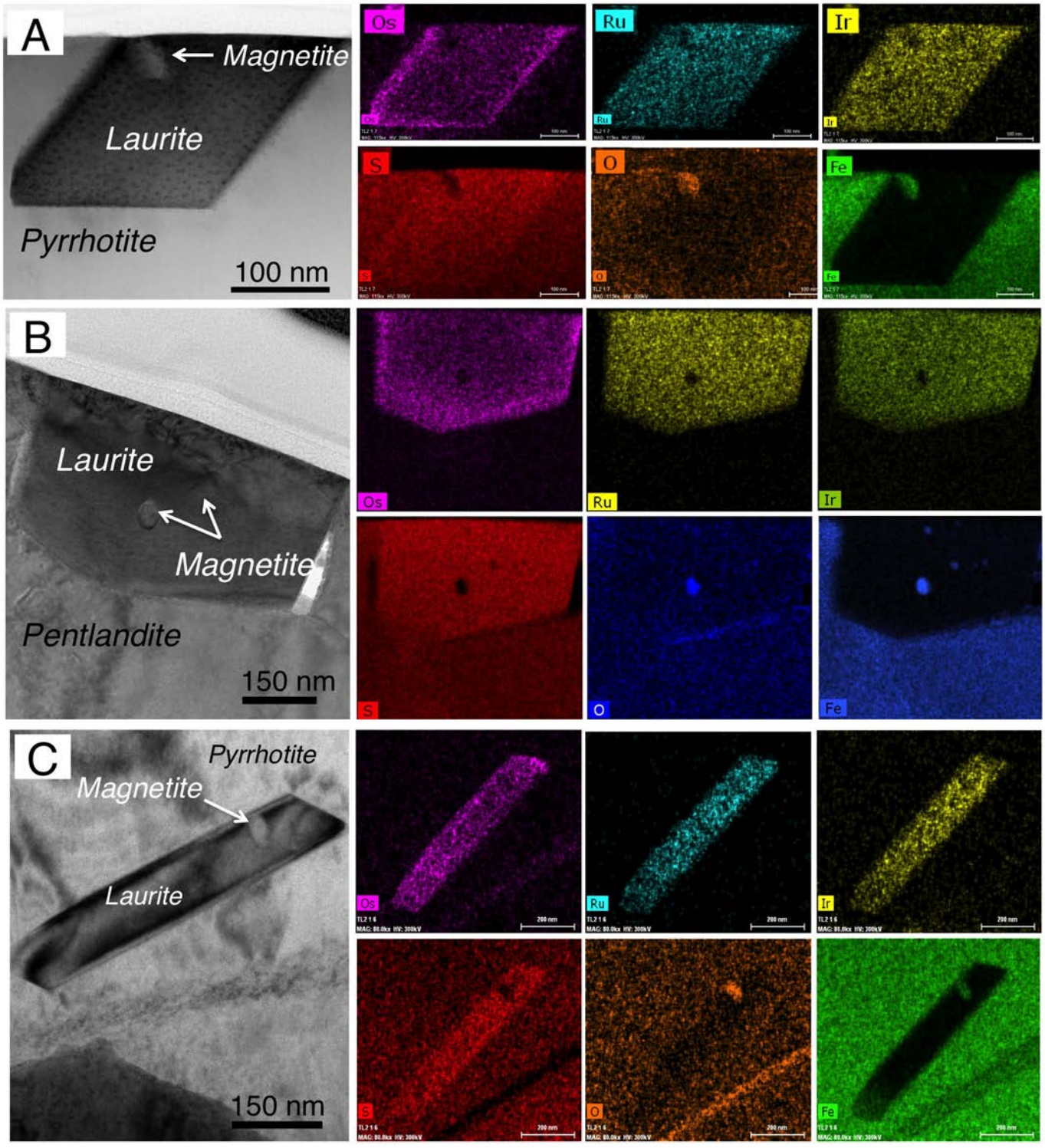

Fig. 4. HAADF-STEM images and associated EDS elemental maps for laurites included in the Tres Lagos PGM-bearing base-metal sulfide bleb shown in Figs. 2 and 3. Each laurite nanoparticle is named A, B and C as in Figs. 3 and 5. Note the Os-rich rim in laurites (A) and (B), the euhedral shape of laurite, and the inclusions of magnetite in laurite.

partial melting and desulfurization of MSS (e.g., Barnes et al., 2016; Luguet et al., 2007; Peregoedova et al., 2004). However, this interpretation is inconsistent with: (1) the well-crystallized nature of laurite, distinctively different from the defective lattice of pyrrhotite, (2) the lack of crystallographic continuity between laurite grains and their host pyrrhotite and pentlandite crystals, (3) the normal zoning of laurite, and (4) the presence of drop-like inclusions of magnetite within laurite. All these observations are consistent with the crystallization of laurite from melt.

Experimental studies indicate that laurite can crystallize directly out from Ni-rich sulfide melts before the crystallization of a MSS (Sinyakova et al., 2019), consistent with its elevated solidus temperature (>1110–1200 °C) in the Ni-Fe-Cu system (Andrews and Brenan, 2002; Brenan and Andrews, 2001). Moreover, the normal zoning exhibited

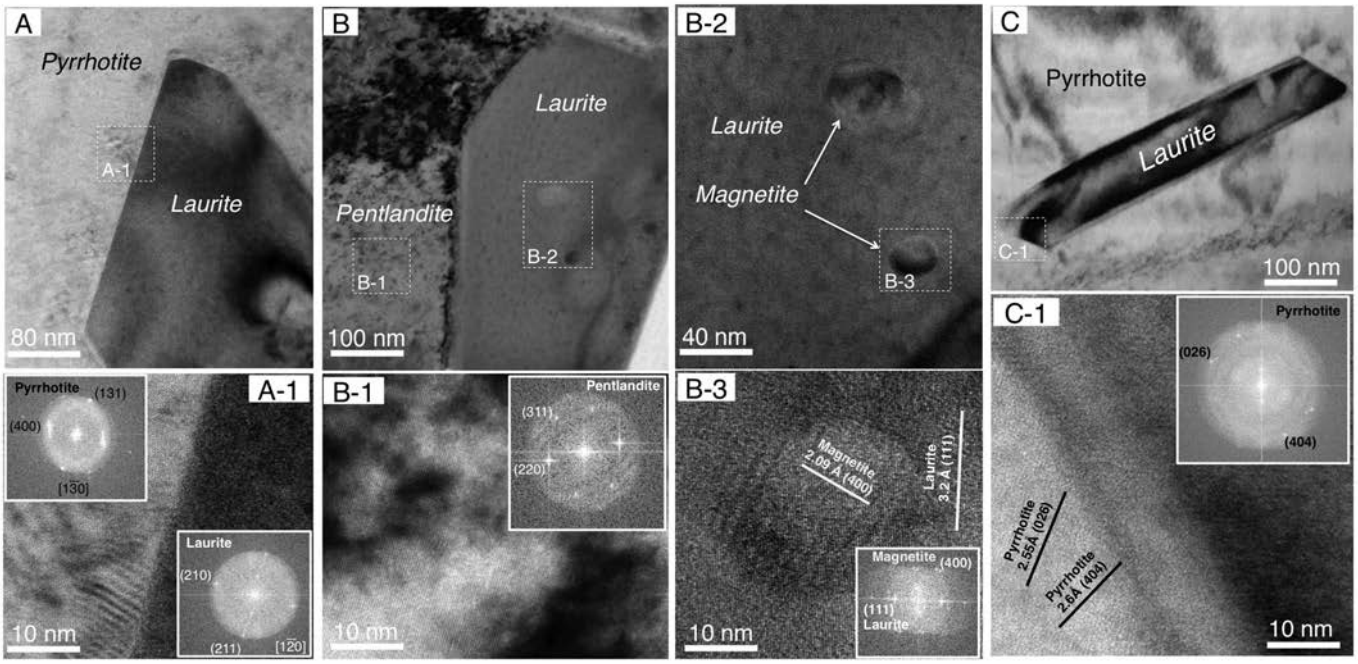

Fig. 5. HRTEM images of the three nano-PGM included in the Tres Lagos PGM-bearing base-metal sulfide blebs shown in Figs. 2, 3 and 4. (A) Low-magnification and (A1) HR-images of the grain boundary between laurite and pyrrhotite. Note the polycrystalline nature of pyrrhotite near the grain boundary. (B, B2) Low-magnification and (B1,3) HR-images of single-crystal of pentlandite (B1) and spherical inclusions of magnetite in single crystal of laurite (B3). (C) Low-magnification and (C1) HR-images of grain boundary between single crystal of pyrrhotite and laurite. Images A1, B1, B3 and C1 include insets of the Fast Fourier Transform (FFT) of HR image showing diffraction maxima and Miller indices for the nanoparticles and host sulfide matrices.

by laurite grains (i.e., Os enrichment toward the rim Fig. 4) suggests that they crystallized from a cooling S-poor melt (González-Jiménez et al., 2009). This melt was also able to crystallize Pt—Fe alloys, similar to those observed in several experimental studies (Fleet and Stone, 1991; Fonseca et al., 2017; Peregoedova et al., 2004; Peregoedova and Ohnenstetter, 2002).

The rounded morphology of magnetite inclusions along with the lack of crystallographic continuity relative to the laurite host (Fig. 5-B2-B3; Appendix 5) could instead point to the existence of droplets of Fe-oxide melt(s) during crystallization of laurite. It is well known that at ~1000 °C and oxygen fugacity close to the QFM buffer, partial melting may produce desulfurization of MSS (Jugo et al., 2010). This drop in fS_2 is usually exacerbated as S becomes exhausted in the sulfide, because the metal/S ratios of residual sulfide reach the metal eutectic. The result of these processes could not only be the partial desulfurization of the pre-existing MSS but also its subsequent breakdown (either solid or liquid) and the possible formation of oxysulfide melt. Available experiments for the Fe-O-S system at 900–1200 °C indicate that sulfide-oxide melts are stable over a large temperature interval and at oxygen fugacity ranging from the stability field of iron to levels close and above the QFM buffer at any given pressure. In these experiments, magnetite is frequently included in immiscible sulfide blebs formed at high temperatures from common basaltic melts (Doyle and Naldrett, 1987; Naldrett, 1969; Shinshin et al., 2015). For instance, analogous microtextures to those observed here, with rounded magnetite inclusions within droplets of BMS, have been reported in peridotite xenoliths from the SCLM (e.g., Bishop et al., 1975; Guo et al., 1999), sub-arc xenoliths (e.g., Melekhova et al., 2017) and modern basaltic lavas (e.g., Larocque et al., 2000; Zelenski et al., 2018). These microtextures were ascribed to sulfide-oxide immiscibility at high temperatures. In the scenario proposed above for partial melting of MSS, small fluctuation in fO_2 may have induced sulfide-oxide melt immiscibility giving rise to laurite that mechanically trapped smaller volumes of immiscible Fe-oxide melt concomitant with the crystallization of "residual" MSS. Nevertheless, the mechanism we propose needs additional experiments to determine precisely the phase relationships in the O-S-Fe-Ni system also involving Ru, Os and Ir.

To summarize, the composite sulfide assemblage enclosed in the olivine grain from Tres Lagos consisting of Ni-rich pyrrhotite + pentlandite + laurite + Pt—Fe alloy is likely to have formed as a consequence of S removal from a precursor MSS during partial melting and oxidation at high temperatures. In detail, such a mechanism would imply the magmatic precipitation of laurite and Pt—Fe alloys directly from the melt, rather than an origin by exsolution from solid MSS as commonly suggested in the literature. This mechanism can apply to other laurite and Os-Ir ± Pt-Fe alloy assemblages reported in mantle peridotites associated with residual MSS enclosed in olivine, such as those from the Udachnaya kimberlite in the Siberian Craton (Griffin et al., 2002) and the Lherz Massif (Luguet et al., 2007). Nevertheless, additional TEM analyses are necessary to confirm this hypothesis. Luguet et al., (2007) noted that this type of PGM-BMS assemblage was only present in the most S-poor harzburgite sample from the Lherz massif, which experienced 19–25% of melt extraction. Interestingly, the strongly depleted peridotite from Tres Lagos (sample TL2–1) experienced a minimum of 14–18% partial melting (Tassara et al., 2018).

4.2. Nano-PGM in BMS hosted within metasomatic pyroxene and carbonate-phosphate

The PGM-bearing BMS within metasomatic pyroxenes from Patagonian and Tallante xenoliths studied here also exhibit droplet-like morphology (Fig. 6A-E and Appendix 6), suggesting their mechanical entrapment in molten state. Sulfide droplets likely represent immiscible PGE-bearing sulfide melt(s) that were segregated from the metasomatic silicate melt that precipitated the pyroxene (Andersen et al., 1987; Bockrath et al., 2004a; Gaetani and Grove, 1999; Robertson et al., 2016).

Platinum is exclusively found at the margin of chalcopyrite forming a composite grain with pentlandite and Ni-rich pyrrhotite in Tres Lagos xenolith (Fig. 6A). The reconstructed composition of the sulfide droplet hosting native Pt falls within the compositional mixing line between Ni-

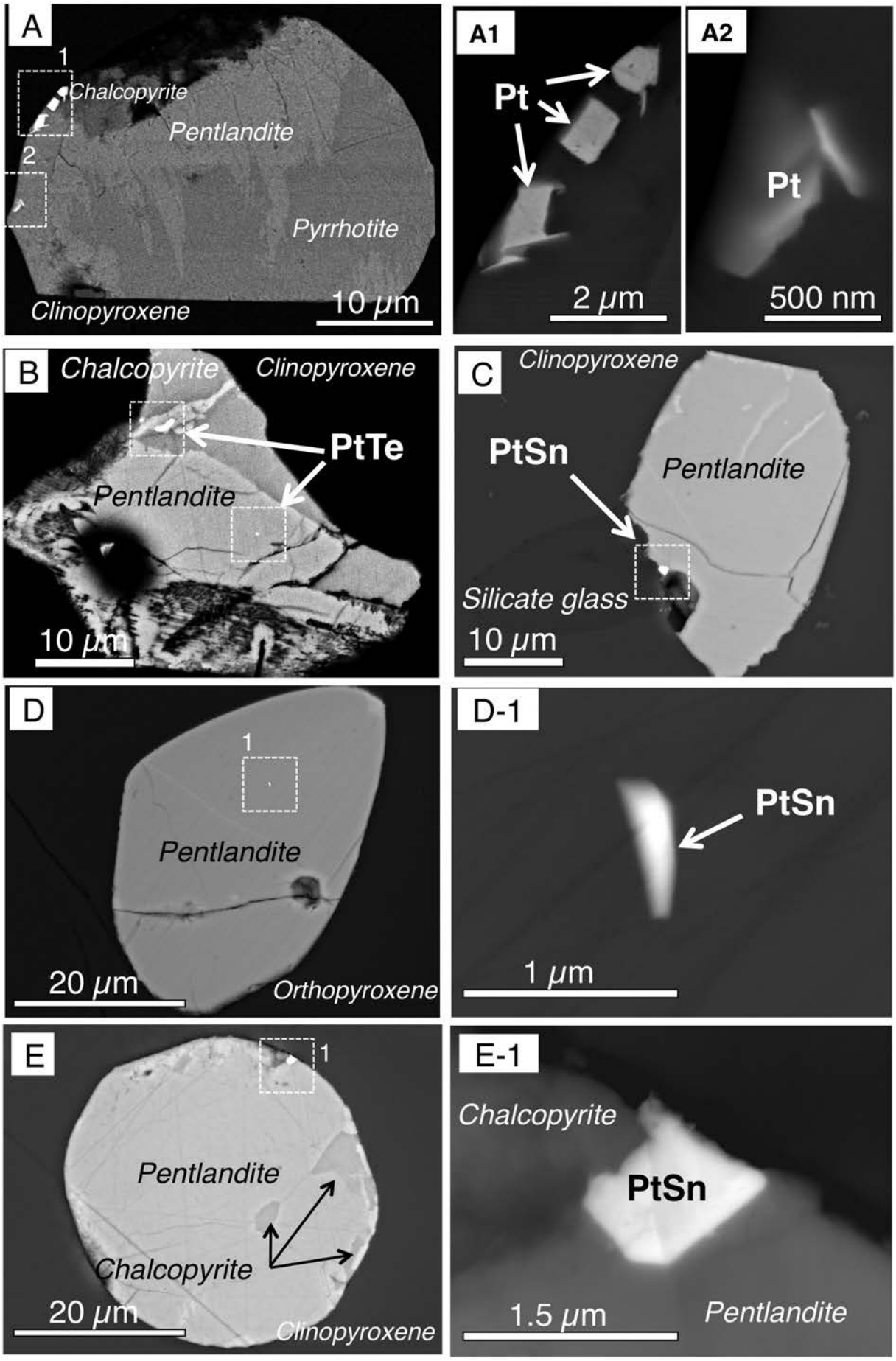

Fig. 6. Backscattered images of the PGM-bearing base-metal sulfide blebs hosted in metasomatic pyroxenes from southern Patagonian xenoliths of Tres Lagos (A, A1 and A2) and Cerro Redondo (B), and from Tallante xenolith from southern Spain (C to E-1).

rich pyrrhotite and pentlandite (Appendix 4), suggesting that this assemblage resulted from the subsolidus re-equilibrium of MSS and the solid products of a coexisting Ni- and Cu-rich sulfide melt. The irregular contacts between pyrrhotite and pentlandite (Fig. 6A) indicate that the Ni excess in the Fe-sulfide formed flame-like pentlandite exsolutions. Canonical views hold that Pt-rich PGM at the margins of mantle BMS originated after sub-solidus transformations of BMS, owing to the limited ability of MSS and Intermediate Solid Solution (ISS) to incorporate Pt in their structures (Fleet et al., 1993; Holwell et al., 2015; Li et al., 1996; Mungall et al., 2005; Peregoedova, 1998). However, the exclusive association of native platinum nanoparticles at the bleb margin of the Tres Lagos xenolith may also indicate a precipitation of the PGM earlier than the BMS. In fact, recent experimental data show that Pt may form its own mineral in Fe-Ni-Cu sulfide melts before the formation of MSS and ISS (Peregoedova and Ohnenstetter, 2002; Sinyakova et al., 2016, 2019). If the sulfide melt lacks semimetals or somehow it was stripped of them, then the formation of Pt metal or alloy is favored (Helmy et al., 2020).

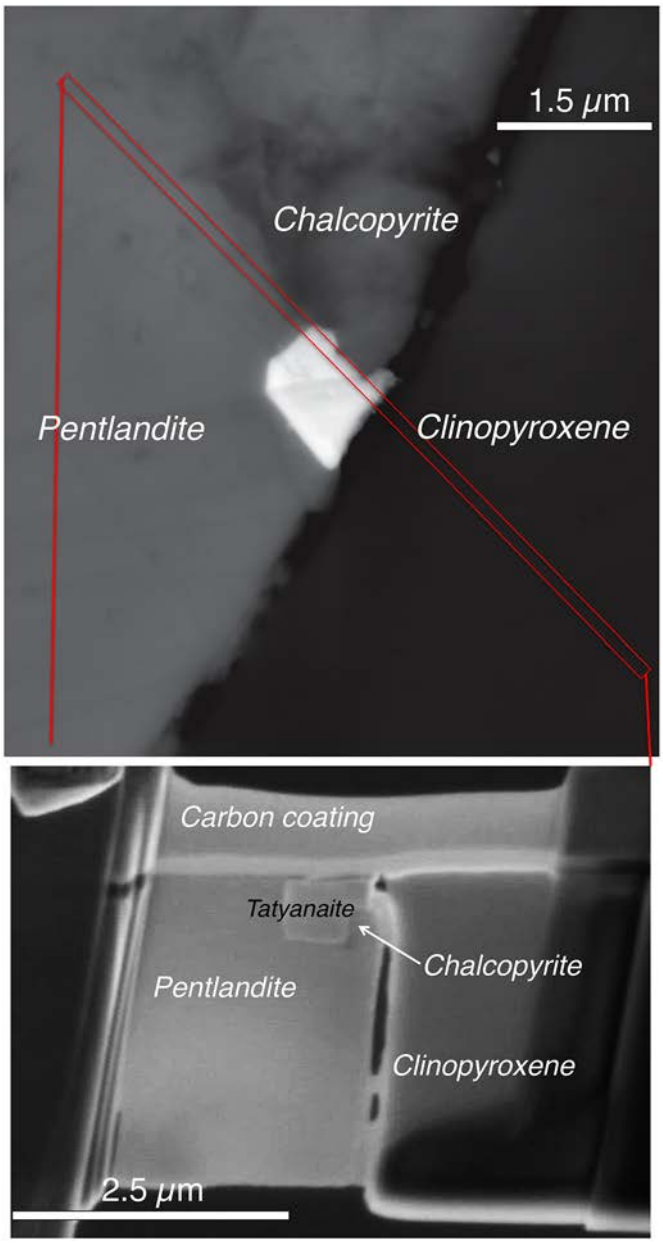

Fig. 7. Back-scattered images of thin-foil sampled from the Tallante PGM-bearing base-metal sulfide bleb shown in Fig. 6E-1. The intersected euhedral grain of nano-PGM is associated with anhedral chalcopyrite at the contact between pentlandite and clinopyroxene.

Pt-Te-Sn compounds were found within isolated pentlandite grains from the Tallante xenoliths (Fig. 6C-D) or at the mutual contacts between pentlandite and chalcopyrite in composite grains from both Tallante and Cerro Redondo xenoliths (Fig. 6B and E). Pentlandite ± chalcopyrite aggregates in metasomatic pyroxenes have usually been interpreted as the product of precipitation of a metasomatic (mobile) Cu-(Ni—Fe)-rich melt formed after incongruent partial melting of a precursor MSS (Luguet and Reisberg, 2016). The first solid product of crystallization of these types of metasomatic Ni- and Cu-rich sulfide melts is the quaternary solid solution consisting of Heazlewoodite [$(Ni,Fe)_{3\pm x}S_2$] solid solution (Hz_{ss}) and ISS [$(Cu_{1\pm x},Fe_{1\pm y})S_2$] (ISS) at 900–850 °C. These could subsequently exsolve pentlandite from Hz_{ss} at ~760 °C and chalcopyrite from ISS below 557 °C (Fleet and Pan, 1994; Kullerud et al., 1969; Peregoedova and Ohnenstetter, 2002). The presence of isolated grains of pentlandite and their sharp contacts with chalcopyrite in the inclusions shown in Fig. 6B-C is consistent with such a fractional crystallization sequence.

Tatyanaite grains (ideally $Pt_9Cu_3Sn_4$) found in Tallante xenoliths exhibit well-developed crystal faces and straight contacts with pentlandite and chalcopyrite, although exhibiting a different orientation of the crystal lattice (Figs. 6E-1, 7, 8 and 9). These observations, together with the uniform distribution of Pt-Te-Sn among both chalcopyrite and pentlandite, suggest that these minerals crystallized from melt before the solidification of the high-temperature precursors of these two BMS. This hypothesis is consistent with the high solidus temperatures of these types of PGM (>1200–1400 °C; Shelton et al., 1981; Kravchenko, 2009) and the experimental results of Sinyakova et al. (2016, 2019), where a wide suite of nano- to micron-sized Pt-Te-Sn minerals crystallized before BMS in a fractionating Cu-rich sulfide melt. This interpretation agrees with the high-temperature origin of pentlandite-hosted moncheite ($PtTe_2$) in pyroxenites of the Ronda ultramafic massif (Gutiérrez-Narbona, 1999). However, this hypothesis contrasts with the origin of a Pd—Sn compound (very likely paolovite, Pd_2Sn) hosted in metasomatic clinopyroxene from Mount Porndon by low-temperature exsolution (Keays et al., 1981).

Our new interpretation that PGM form by high temperature crystallization prior to their hosting BMS may also apply to the micron-sized cooperite (PtS) intimately associated with chalcopyrite in pyrrhotite-pentlandite-chalcopyrite-carbonate composite blebs reported by Hughes et al. (2016) in xenoliths from the marginal cratonic Hebridean Terrane in Scotland. Those PGM were also attached to BMS suggesting the crystallization of the Pt-sulfide from the Cu-rich sulfide melt before ISS (precursor to chalcopyrite) segregation. Several experiments in the Pt-Ni-Fe-Cu-S system have shown that cooperite can crystallize directly out from sulfide melts of the three ternary subsystems Fe-Ni-S, Cu-Fe-S and Cu-Ni-S at >900 °C (Makovicky, 2002; Peregoedova and Ohnenstetter, 2002; Sinyakova et al., 2016).

Alard et al. (2011) and Delpech et al. (2012) also proposed carbonate and phosphate-rich metasomatism to explain the origin of Pt-Pd-As (including sperrylite, $PtAs_2$) and Pt-Te-Bi minerals that they identified in composite sulfide blebs of pyrrhotite ± pentlandite ± cubanite± carbonate ± phosphate found in the Montferrier xenoliths and in dunite xenoliths from Kerguelen. Interestingly, these Pt-Pd-rich Te-Bi-As minerals reported in xenoliths were also found attached to sulfide blebs or at the mutual contact between the BMS. A renewed look of this micro-textural relationship provides an alternative scenario for the formation of all these Pt-Pd-rich Te-Bi-As minerals involving their direct precipitation from sulfide melts at high-temperatures. The nucleation of these types of PGM directly from the sulfide melt is enhanced whenever PGE are dissolved in the liquid as PGE + semimetal complexes (Helmy et al., 2020; Sinyakova et al., 2016). These complexes are formed by the clustering of hundreds of atoms of PGE + semimetal, which could help to overcome the kinetic barrier of nucleation (due to low concentration

of PGE in melt) of the nano- and micron-sized PGM, thus acting as seeds for the crystallization of larger microscopic BMS (Helmy et al., 2013; Junge et al., 2015). Alternatively, these Pt-Pd-rich Te-Bi-As minerals could crystallize from nano-to micron-scale droplets of PGE-bearing Te-Bi-As melts immiscible with the sulfide droplets that they are in contact. This process may take place at >1000 °C, as observed in recent experimental works (Anenburg and Mavrogenes, 2020; Helmy and Botcharnikov, 2020).

4.3. Nano-PGM associated with BMS entrained in silicate glasses

Platinum nanoparticles are relatively common in pentlandite blebs entrained in silicate glasses from the locality of Gobernador Gregores in southern Patagonia (Fig. 10A) and the La Breña in Central Mexico (Figs. 10B-C and 11F-G). The identification of oxy-hydroxides replacing some of the Mexican pentlandite grains suggests that mantle sulfides experienced in situ partial desulfurization followed by oxidation, probably under conditions of weathering of the host silicate glass at near-surface temperatures (Szabó and Bodnar, 1995). O'Driscoll and González-Jiménez (2016) interpreted similar Pt—Fe nanoalloys located at edges of partly desulfurized MSS in mantle xenoliths from Calatrava (southwestern Spain) as PGE that, initially dissolved in BMS, were locally remobilized when BMS experienced desulfurization and oxidation.

However, many other mantle xenoliths from Gobernador Gregores and Cerro Redondo contain nanoparticles (~20–80 nm) of Pt-rich alloys and arsenides hosted in unaltered BMS (pentlandite, millerite and MSS) entrained within silicate glasses interstitial to the silicate mineral assemblage (González-Jiménez et al., 2019). The investigation of four of these Pt-rich nanoparticles hosted in two pentlandite droplets from Gobernador Gregores (sample GG-14) and Cerro Redondo (sample CR-07) by González-Jiménez et al. (2019) using FIB/HRTEM revealed that these nanoparticles consist of polycrystalline aggregates <10 nm that are randomly oriented relative to their sulfide host matrices. Since Pt-rich nanoparticles usually consist of aggregates formed by smaller crystals (<10 nm), their formation may be have resulted from clustering of smaller Pt nanoparticles in sulfide melts prior to the crystallization of their hosting BMS (González-Jiménez et al., 2019). This interpretation is consistent with phase relations in the Pt-Fe-Ni-S system predicting the formation of Pt-rich alloys with Fe- and Ni-bearing sulfide melts in equilibrium at >1100–1300 °C (e.g., Majzlan et al., 2002) and experiments reviewed by Pruseth and Palme (2004) where Pt and Pt—Fe nanoalloys also formed in Fe-rich sulfide melts at fO_2 defined by the QFM buffer.

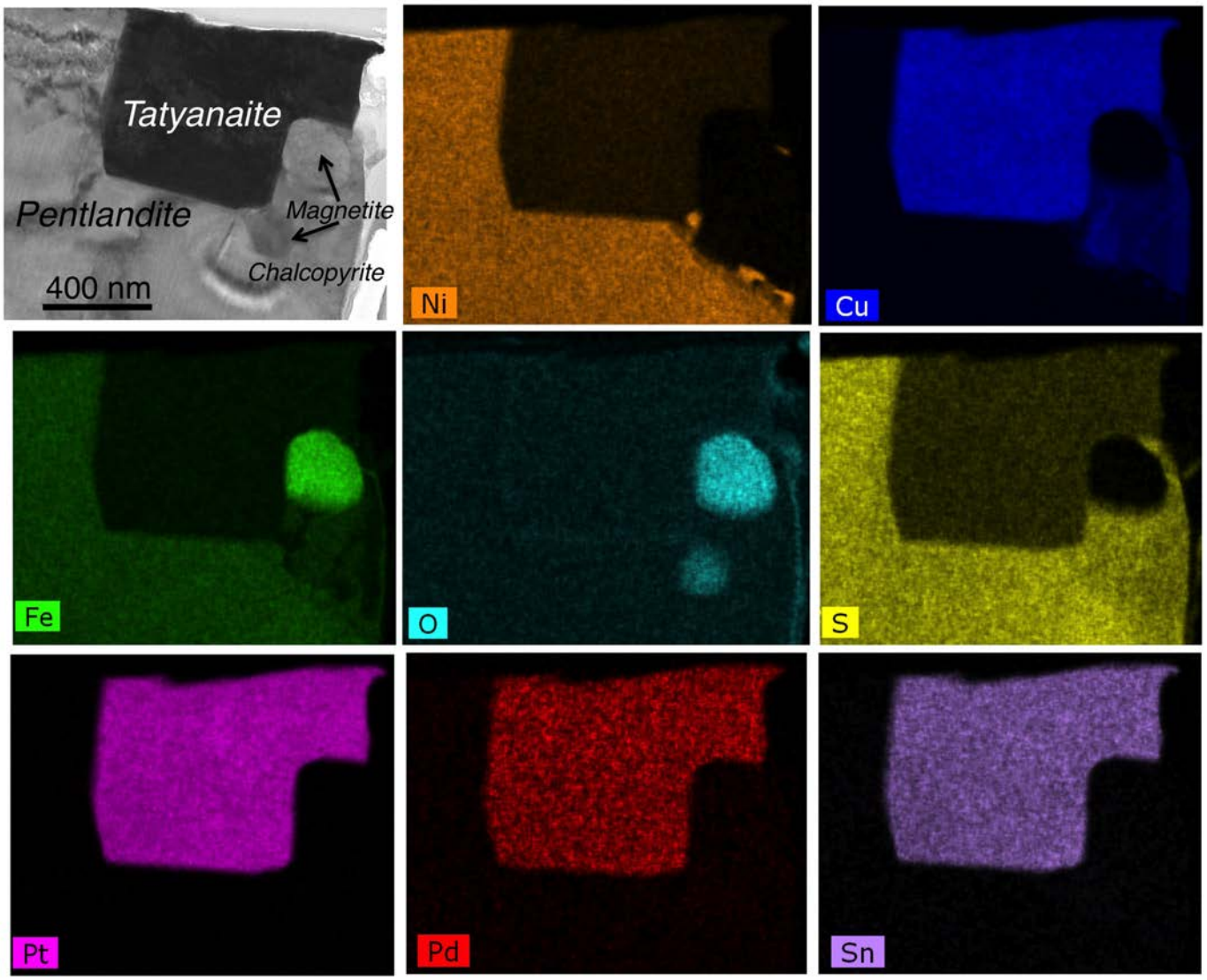

Fig. 8. HAADF-STEM image and EDS elemental mapping of the Pt—Sn nanoparticle, magnetite, chalcopyrite and hosting pentlandite from Tallante xenolith shown in Fig. 6E-1.

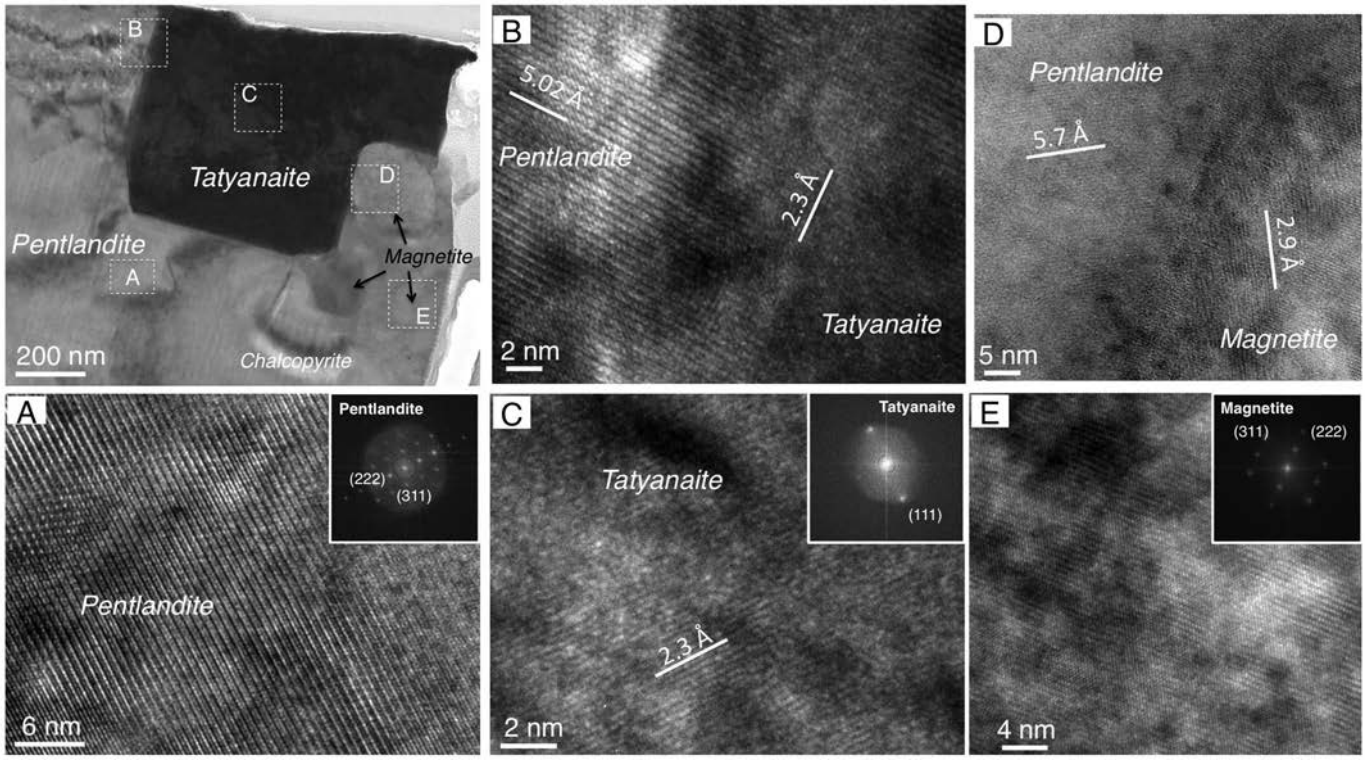

Fig. 9. Low-magnification and high-magnification HRTEM images and associated Fast Fourier Transform (FFT) of HR image of the nano-PGM the Tallante PGM-bearing base-metal sulfide bleb shown in Fig. 6E-1 (B) HRTEM image of the gran boundary between single crystals of pentlandite (see image A) and tatyanaite (see image C). (D) HRTEM image of grain boundary between pentlandite and magnetite; note the misorientation and defects between these two minerals. (E) HR image of single crystal of magnetite.

The above discussion points out that, although the formation of Pt nanoparticles in BMS located within interstitial silicate glasses in mantle xenoliths is possible after oxidative weathering of PGE-bearing BMS (e.g., Fig. 10A-D), many of these could also represent primary phases formed from sulfide melts migrating through the SCLM as droplets entrained in silicate (basaltic) melts. As noted above, the precipitation of native Pt or Pt-rich nanoalloys before BMS is promoted whenever ligands such as Te, As, Sb, Bi are not available in the sulfide melt (e.g., Piña et al., 2012). In contrast, Te and/or As, when available in the melt could form nanograins of Pd—Te (possibly merenskyite, $PdTe_2$) as those observed in the pentlandite-chalcopyrite grain shown in Fig. 10E, and Pt—As (possibly sperrylite $PtAs_2$) as those at contact between pentlandite and millerite, shown in Fig. 10F-G.

A sulfide bleb entrained in the interstitial glass of xenoliths from Gobernador Gregores also contains Pd—S compounds (possibly braggite, PdS) located at the contact between pyrrhotite and pentlandite (Fig. 10D and D-1; sample GG-01). This sulfide bleb was originally transported in a silicate melt that crystallized at 1064–998 °C (Appendix 1). This pentlandite-pyrrhotite assemblage likely formed after the subsolidus re-equilibration of a precursor MSS that crystallized at high temperatures from a sulfide droplet rich in Ni and Fe and depleted in Cu. Experiments show that Pd is relatively incompatible in MSS relative to Cu—Ni rich sulfide melts ($D_{Pd}^{mss/sulf} = 0.005–0.44$; Fleet et al., 1993; Li et al., 1996; Mungall et al., 2005; Brenan et al., 2016). Therefore, pentlandite derived from re-equilibration of MSS is expected to contain very little Pd. However, other experimental work (e.g., Makovicky et al., 1986) has shown that at high temperature (900 °C) MSS can dissolve up to 11 wt% Pd, but when temperature falls the solubility of Pd decreases dramatically (≤0.4 wt% at 500 °C). The results of these experiments indicate that, upon cooling of MSS, Pd should enter in the structure of pentlandite instead of MSS. This inference is consistent with the fact that Pd-rich pentlandite coexists with Pd-poor pyrrhotite in several Ni—Cu deposits (Barnes and Dare, 2010; Piña et al., 2012) and mantle xenoliths (Luguet and Reisberg, 2016; Tassara et al., 2018). The observation of braggite at the contact between pentlandite and pyrrhotite may suggest that Pd was initially incorporated into MSS and then partitioned into pentlandite at ≤610 °C. However, other experiments have shown that solid PdS may crystallize from sulfide melt in equilibrium with MSS below 912 °C in the Pd-Fe-S system (Makovicky et al., 1988; Makovicky and Karup-Møller, 1993) and at 900 °C in the Pd-Ni-S systems (Karup-Møller and Makovicky, 1993). Additional studies of the Pd-Fe-Ni-S system (Makovicky et al., 1990; Makovicky and Karup-Møller, 1993) also showed the co-crystallization of PdS and MSS [$(Fe, Ni)_{1-xS}$] at 900 °C, with the association PdS-MSS still stable down to 725 °C, but decomposing at lower temperature into PdS ± pentlandite ± pyrrhotite (Makovicky, 2002). On the basis of the aforementioned experimental studies, we suggest that natural PdS, like those identified in the BMS bleb from the Gobernador Gregores xenolith, may have also formed at magmatic temperatures preceding the formation of the enclosing MSS. Nevertheless, additional TEM studies are required to confirm this hypothesis.

4.4. Nano-PGM embedded in silicate glasses

Mantle xenoliths from Gobernador Gregores and Cerro Redondo contain abundant nano-sized particles of Pt-rich alloys dispersed within interstitial silicate glasses (e.g., Fig. 3a-b in González-Jiménez et al., 2019). Frequently, these Pt-rich alloys are adhering to co-genetic oxides (ilmenite or Cr-Spinel) also embedded within the silicate glass. In fact, experimental studies have shown the crystallization of Pt and Pt—Fe nanoparticles at >1000 °C from basaltic melts buffered with fO_2 near the QFM buffer often in presence of Cr-Fe-Ti oxides (Anenburg and Mavrogenes, 2016; Médard et al., 2015). The results of the experiments also show that, in alkaline melts at fO_2 near the QFM buffer, the crystallization of oxides (ilmenite or Cr-spinel) from the parental alkaline melt may locally lower fO_2 enough to promote the precipitation of Pt

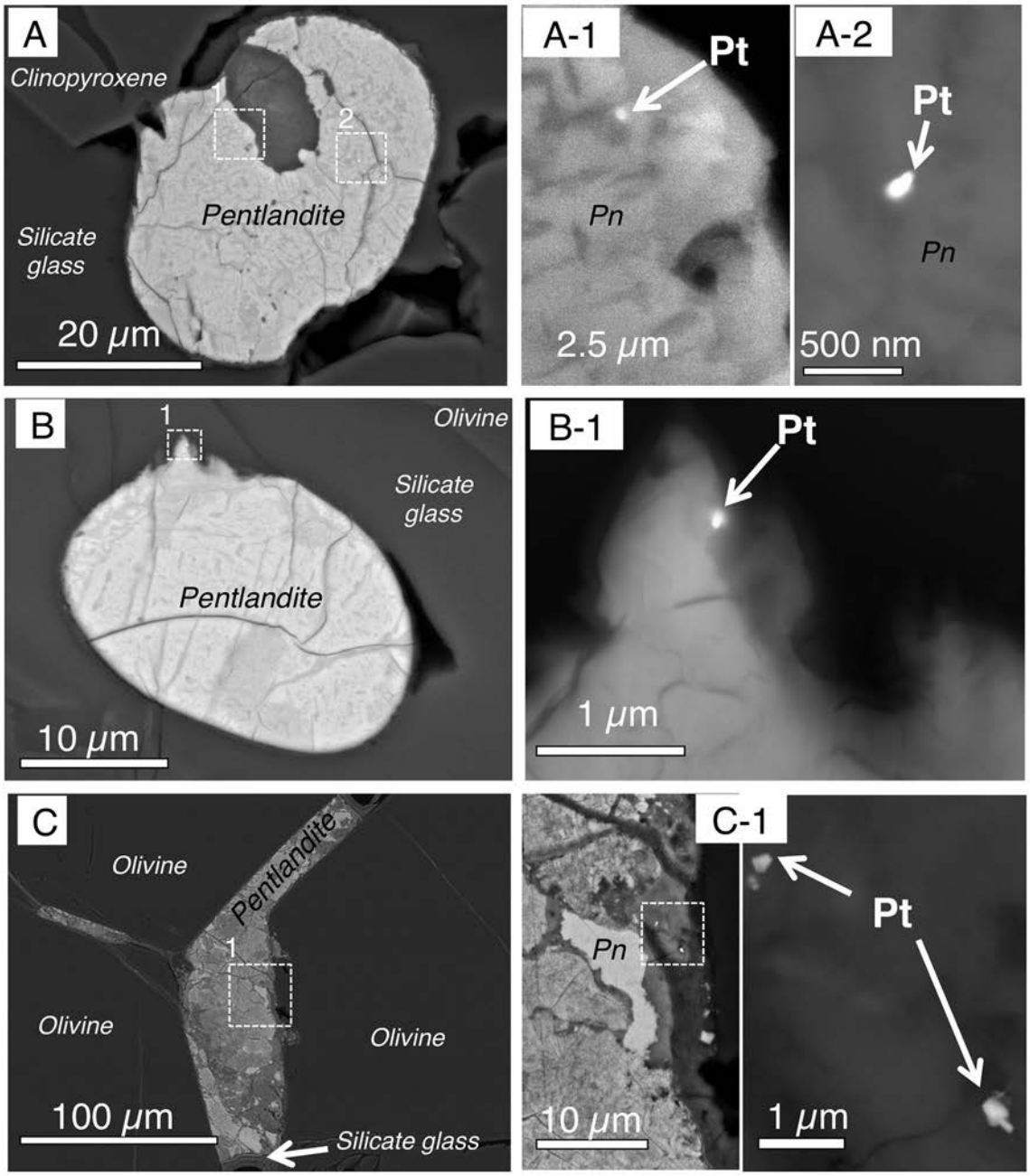

Fig. 10. Backscattered electron images of the PGM-bearing base-metal sulfide blebs hosted in metasomatic interstitial glass in mantle xenoliths (this study). The suite of nano-PGM include: native Pt in the Patagonian locality of Cerro Redondo (A to A2) and the Mexican locality of La Breña (B to C-1), PdS (possibly braggite) and Pt—As (possibly sperrylite) in Cerro Redondo (D-G) as well as Ru—S (possibly laurite) in Cerro Redondo and Pali-Aike (H-J) also in Patagonia.

dissolved in the basaltic melt as Pt-rich nanoparticles (e.g., Anenburg and Mavrogenes, 2016). Notably, Pt—Fe alloys (~$Pt_{0.83}Fe_{0.17}$) have been reported to be included in Cr-spinel from picritic lavas from the active Ambae volcano, in Vanuatu (Fig. 1; Kamenetsky et al., 2015 and references therein), providing an additional case in nature for the direct precipitation of Pt-rich alloys from silicate magmas.

On the other hand, two discrete grains of a Ru—S compound (possibly laurite, RuS_2) were identified as isolated crystals embedded in the interstitial glass of mantle xenoliths from southern Patagonia in Cerro Redondo (replicate sample CR-08) and Pali-Aike (sample PA-LA7) (Fig. 10H-J). These two laurites could be interpreted in two ways: (1) as xenocrysts physically entrained by metasomatic silicate melt (now is preserved as a quenched glass) or, (2) minerals crystallized from such metasomatic silicate melt. The first hypothesis implies that these PGM were residual grains after the complete consumption of precursor BMS during melting or melt-rock reactions taking place in the mantle peridotite (e.g., Fonseca et al., 2012). The second possibility is sustained by several experimental and empirical results, showing that laurite may crystallize as the earliest liquidus phase at ~1200–1300 °C from sulfide-undersaturated basaltic melts (Andrews and Brenan, 2002; Bockrath et al., 2004b; Brenan and Andrews, 2001). Experimental work on simple basalt analogues in the system SiO_2-Al_2O_3-MgO-CaO-Cr_2O_3 (CrMAS), together with thermodynamic consideration of the relevant equilibria, suggest that there is a "window" in the fS_2–fO_2–T space in which laurite may precipitate directly from

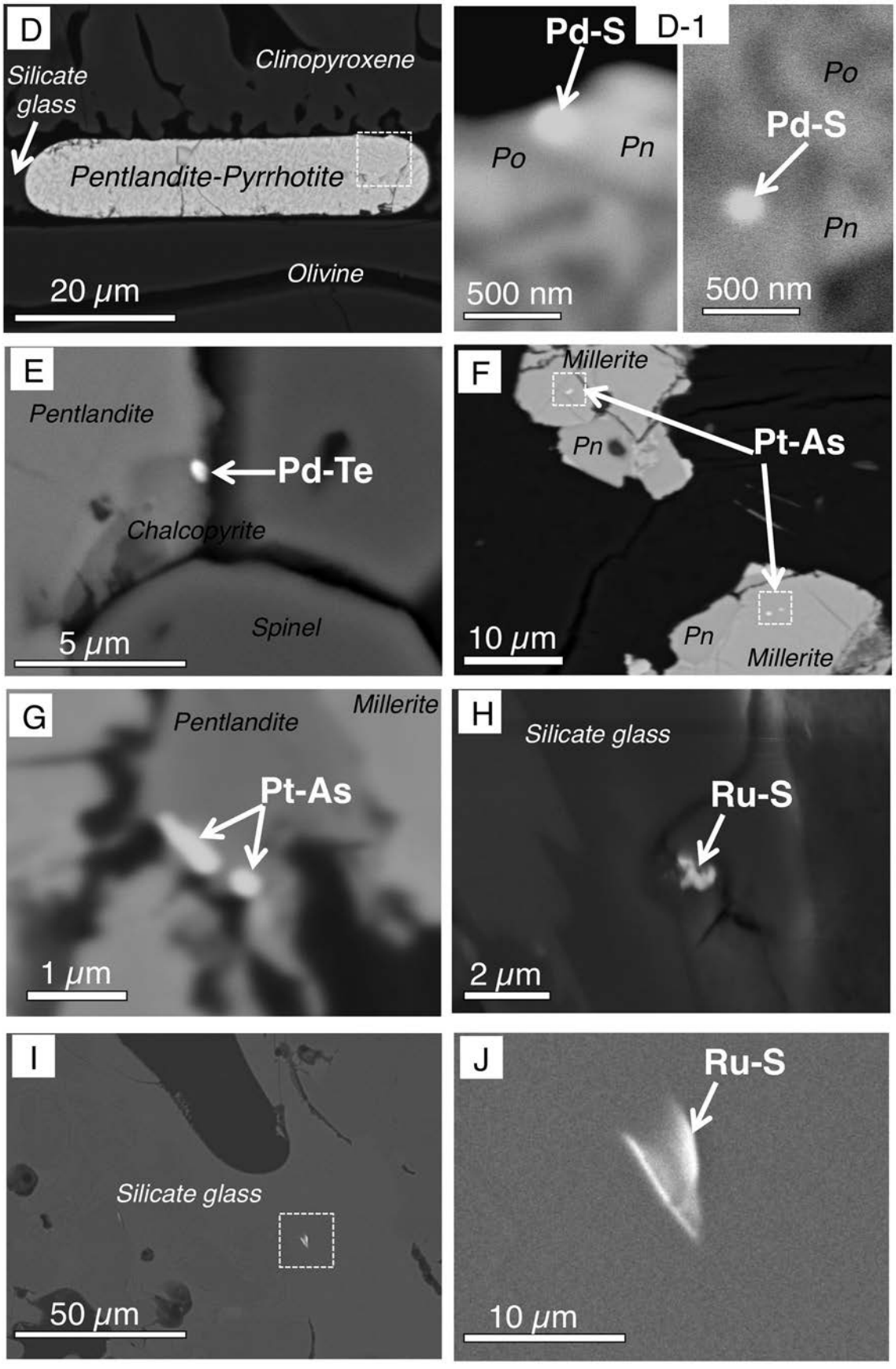

Fig. 10 (*continued*).

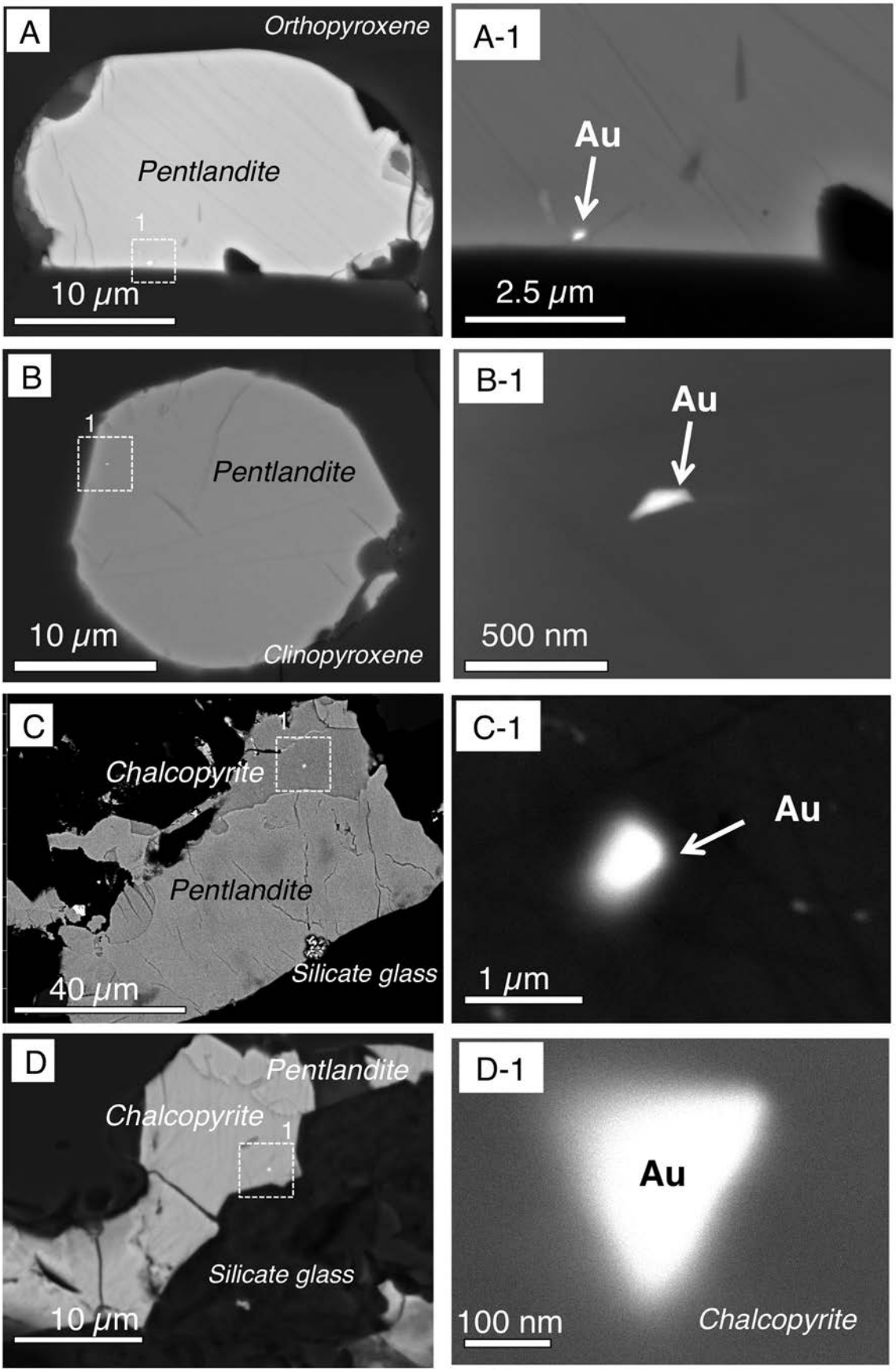
A
Orthopyroxene
Pentlandite
1
10 μm
A-1
Au
2.5 μm
B
1
Pentlandite
10 μm
Clinopyroxene
B-1
Au
500 nm
C
1
Chalcopyrite
Pentlandite
Silicate glass
40 μm
C-1
Au
1 μm
D
Pentlandite
Chalcopyrite
1
Silicate glass
10 μm
D-1
Au
100 nm
Chalcopyrite

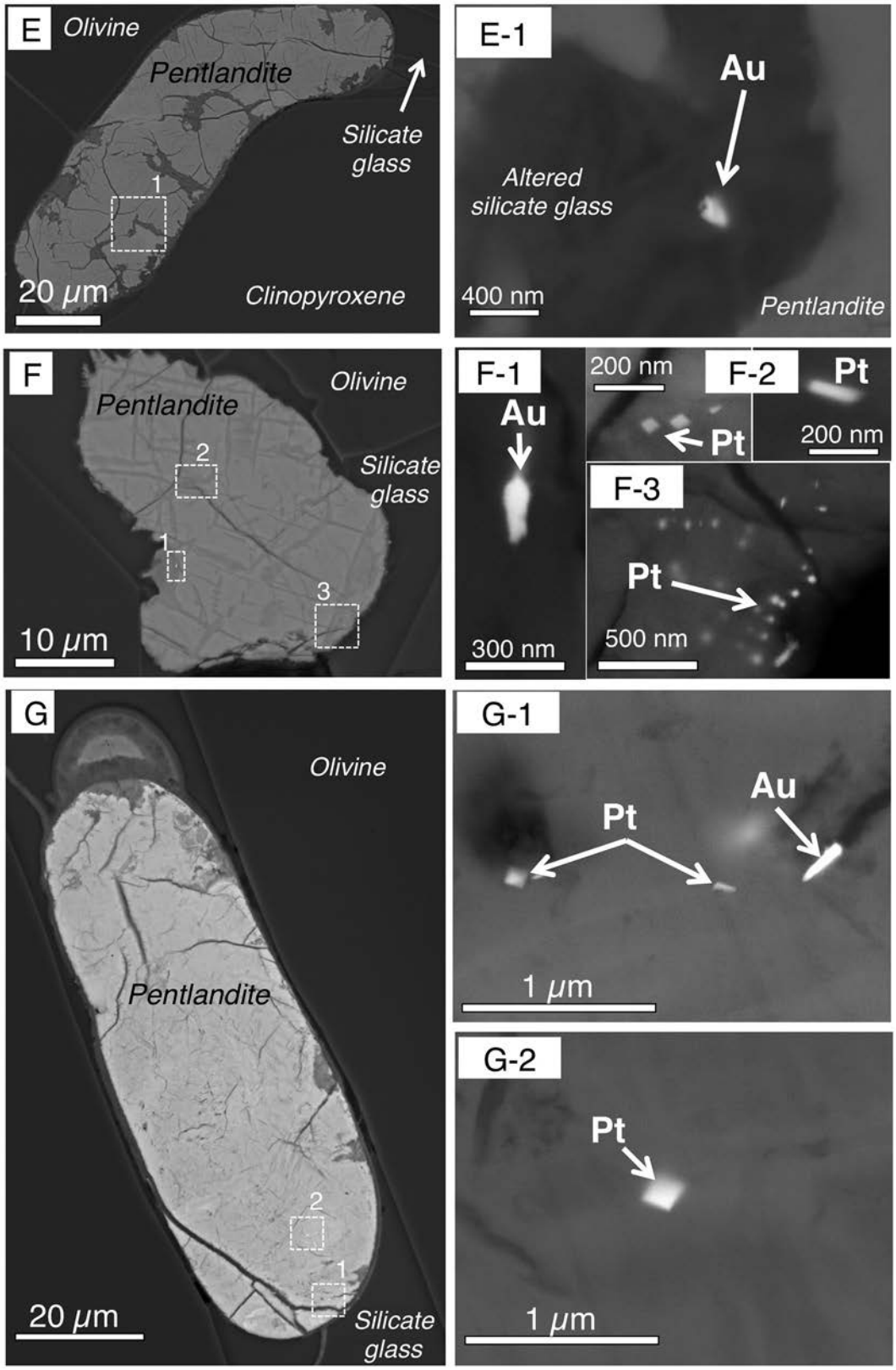

Fig. 11. Backscattered electron images of the Au-bearing base-metal sulfide blebs hosted in metasomatic interstitial glass in the mantle xenoliths from Tallante in southern Spain (A to B1), Cerro Redondo in Patagonia (C to D-1) and La Breña in central Mexico (E to G-2).

silicate melt w. The size of this window is a function of fO_2 and to a lesser extent of the FeO content in the silicate melt (Andrews and Brenan, 2002; Bockrath et al., 2004b). Thus, magmatic laurite can crystallize more easily from oxidized silicate melts with fO_2 higher than $\Delta QFM = -1.5$, conditions that apply to the late infiltrating melt (i.e., the glassy veins) that bear the laurites in the Cerro Redondo and Pali-Aike

peridotites (Tassara et al., 2020). However, some experiments have shown that a Ru metal nugget formation might precede laurite crystallization in melts, which could form when these Ru nuggets n reacted with sulfur once fS_2 increased in the silicate melt (Bockrath et al., 2004b). This mechanism has been related to the crystallization of Fe-Ti-Cr-oxides (ilmenite and Cr-spinel) and/or silicates (e.g., secondary pyroxene or olivine) that promotes local perturbations in fO_2 at their melt-solid interfaces necessary for the precipitation of Ru (also Os and Ir) as metallic nanoparticles. As noted above, this is a feasible scenario for the cases of Cerro Redondo and Pali-Aike in southern Patagonia where the interstitial glass contains frequent newly-formed oxides and silicates.

4.5. Transport and precipitation of gold nanoparticles in magmas migrating through the SCLM

Gold-bearing millerite/pentlandite ± chalcopyrite composite grains have been found within metasomatic pyroxenes from the Tallante xenoliths (southeast Spain) (Fig. 11A-B) and entrained within interstitial glass from Cerro Redondo xenoliths in southern Patagonia (Figs. 11C-

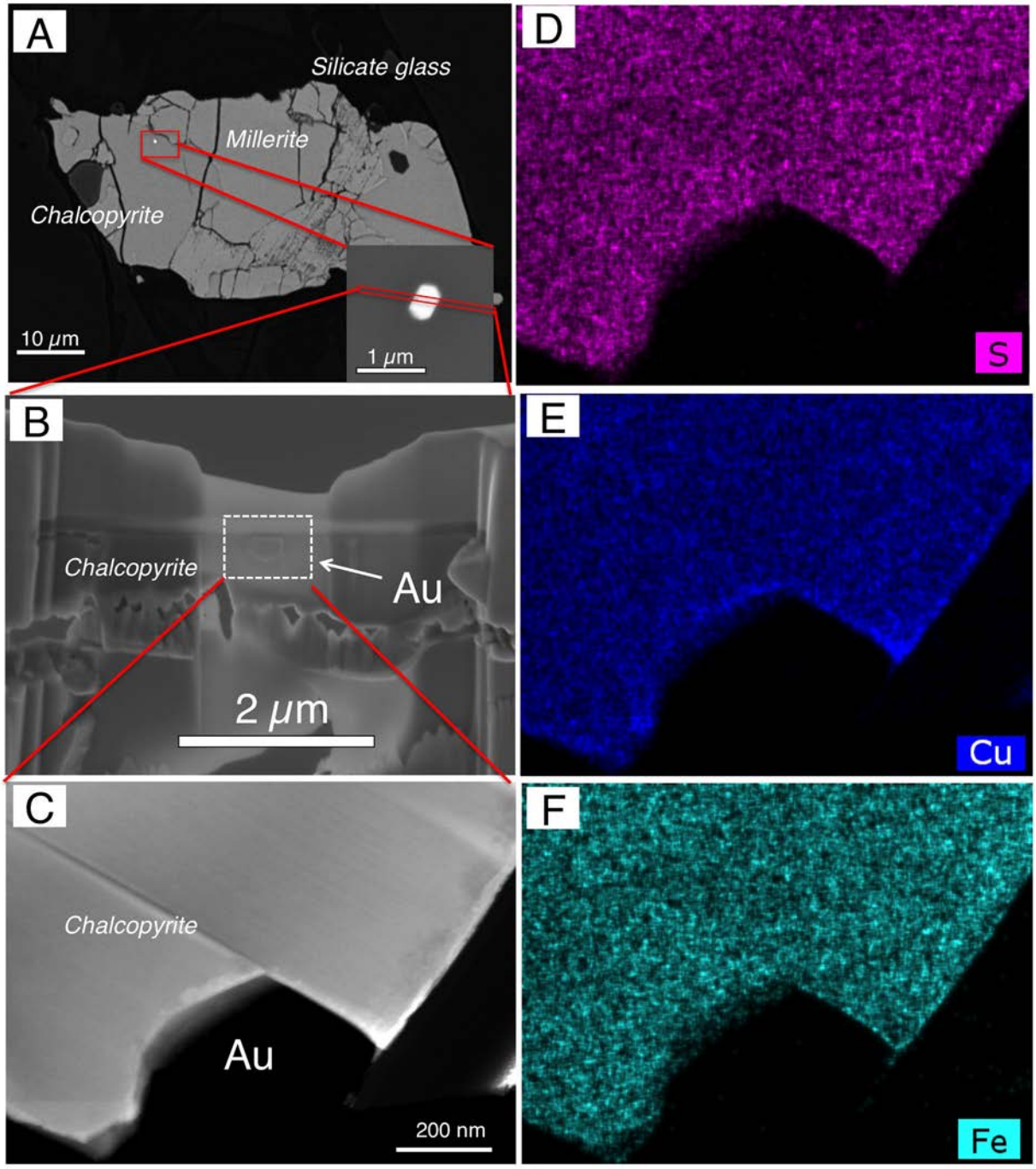

Fig. 12. (A) Back-scattered electron images of a PGM-bearing base-metal sulfide bleb identified by Tassara et al. (2017) in a xenolith from the Patagonian locality of Cerro Redondo (Fig. 2b-c in the cited paper); a thin-foil was sampled from this sulfide bleb in B. Image C is a HAADF-STEM image of the thin-foil damaged during thinning. The Au NP was lost. Note the euhedral shape of the Au NP in image A and B.

D and 12). These composite sulfide grains likely correspond to the solid products of Ni-Cu-(Fe) sulfide melts segregated from, or transported by, the metasomatic silicate melts at upper mantle conditions (Tassara et al., 2018). A similar origin can be assumed for the partly altered pentlandite from La Breña in central Mexico (Fig. 11F-G) and Matsoku in northern Lesoto (Appendix 6).

Experiments in the Fe-Ni-Cu-S system indicate that gold is incompatible in MSS but has strong preference for Cu-rich melts (Li and Audétat, 2013; Mungall et al., 2005). Upon crystallization of Cu-rich melts, gold may reach concentrations up to thousands of ppm in ISS, but it is almost insoluble into low-T phases such as chalcopyrite and pentlandite (Djon and Barnes, 2012; Piña et al., 2012). Besides, some empirical results have shown that gold may not partition to ISS if it becomes sufficiently enriched in the Cu-(Ni—Fe)-rich melts to form its own minerals (e.g., Barnes et al., 2006; Holwell et al., 2015). In the xenoliths studied here, euhedral Au nanoparticles with crystal habits typical of the cubic system are located in both chalcopyrite and pentlandite (e.g., Figs. 11D and 12). This suggests their potential formation before the crystallization of the high-temperature precursors of the hosting BMS. In fact, the recent experiments by Sinyakova et al. (2019) indicate the crystallization of gold at high temperatures (> 1000 °C) from Ni-Cu-Fe sulfide melts before BMS. This interpretation could also be consistent with the presence of euhedral crystals of gold in millerite (Fig. 12) as well as of clusters of native Au nanoparticles in the chalcopyrite portion of pentlandite-chalcopyrite grains from the interstitial glass of Cerro Redondo xenolith (see Fig. 2h in Tassara et al., 2017).

It is important to note that the interstitial silicate glass of Cerro Redondo xenoliths also hosts several isolated gold particles not directly associated with BMS (see Fig. 2f in Tassara et al., 2017). Decreasing pressure or increasing fO_2 during the melt-rock reaction associated with silicate melt infiltration would increase the S solubility (Jugo et al., 2010; Mavrogenes and O'Neill, 1999), promoting the partial dissolution of the Ni—Cu sulfide blebs into the silicate melt and the release of the gold particles (Tassara et al., 2020). If liberated to the surrounding silicate melt, the high Au solubility in the silicate melt would result in the partial resorption of these particles. This scenario explains well why gold particles are euhedral when included in the sulfides, but it is anhedral when included in the interstitial silicate glass, as observed by Tassara et al. (2017).

Alternatively, Au particles found in these BMS and silicate glasses could correspond to xenocrysts or particles precipitated earlier from the silicate melt. Gold solubility in silicate melts increases as the content of alkali metals and fS_2 in the system both increase (Li et al., 2019), and if S is present as both reduced (S^{2-}) and oxidized (S^{6+}) species (Li and Audétat, 2013). In this scenario, the segregation of immiscible Ni—Cu sulfide melts or the incorporation of sulfur dissolved in the silicate melt into the crystallizing Ni—Cu sulfides would decrease gold solubility, triggering its precipitation.

Interestingly, Zelenski et al. 2017 and Kamenetsky and Zelenski (2020) have reported several particles (<100 nm to 3 μm, with the majority falling in the range of 200–500 nm) made up of sulfides, and alloys of Pd, Pt, Au, Pb, and Bi within sulfide melt inclusions in primitive olivine phenocrysts from the Tolbachik arc volcano, Kamchatka. These gold and PGM particles were found within sulfide matrices or, more commonly, at the contacts between the different BMS (i.e., MSS-ISS, pentlandite-ISS), indicating the early-magmatic origin of the PGM and gold particles. Micron-sized particles of native gold have also been documented in the glassy groundmass of lamproite dikes from El Tale in southern Spain (Toscani, 1999) and basanite lavas from Hawaii (Sisson, 2003) (Fig. 1), suggesting direct crystallization of gold from alkali-rich silicate magmas. Moreover, Zhang et al. (2006) have also reported a bleb of pure Au (~30 μm in diameter) enclosed in a fresh olivine phenocryst from picrites in southwestern China. This Au bleb was interpreted to be a xenocryst from the deep mantle transported to shallow depths by a rising plume and then captured by picritic melts (Zhang et al., 2006).

All the observations described above support the hypothesis of a magmatic origin of gold minerals in the SCLM. These gold particles could be interpreted as primary precipitates from the metasomatic (mobile) Ni-Cu-(Fe) sulfide melt, or even silicate melts. However, it cannot explain the micron-sized grains of native gold found in Lherz peridotites (also containing PGM; Lorand et al., 2010). According to Lorand et al. (2010), these gold particles were detected inside cracks or alteration contacts between pentlandite and chalcopyrite. Furthermore, gold nanoparticles (including native gold, novodneprite and anyuiite) identified by Ferraris and Lorand (2015) included in olivine from another Lherz peridotite are better explained by circulation of Au-rich fluids during a secondary growth phase of olivine grains. As noted above, a process of plastic deformation enhanced the formation of edge dislocations within olivine grains and thus, the circulation within them of Au-enriched fluids (Ferraris and Lorand, 2015).

5. Conclusions and broader implications

The observations provided in this paper highlight that HSE are not only incorporated as solid-solution trace-metals into mantle BMS but also as discrete nano- to-micron sized minerals and particles. The microstructural position of HSE-bearing minerals within mantle peridotites is an important constraint to define whether they resulted from partial melting or metasomatic processes. Whereas HSE-bearing minerals enclosed in residual olivine, or located along interstices of primary minerals, are regarded to have crystallized as a result of melt extraction events, those associated with metasomatic phases (pyroxenes, carbonate-phosphate and interstitial silicate glasses) are formed after melt percolation and melt-peridotite interactions. The formation and stability of these mineral particles predominantly depends on temperature, fO_2, and the activities of chalcogens such as S, As, Te, and Bi in melts. We show that a whole suite of nano-to-micron-sized discrete minerals of the HSE (alloys, sulfides, arsenides, bismuthides, tellurides) can be stable in both silicate and sulfide melts present in the SCLM. The origin of PGM and gold minerals in these textural positions is often related to their direct crystallization from melts in the mantle rather than exsolution from host minerals. Importantly, we highlight that the mechanism of fractionation and transport of the HSE in mantle melt is not exclusively related to their chemical high sulfide/silicate partition coefficients, because nanoparticles and nanomelts may also exert a key role. The latter may impose a significant fraction of the HSE in silicate and sulfide mantle melts. This conclusion is not only sustained by our observation of HSE-bearing nanominerals and nanoparticles in the interstitial glass of many mantle rocks but also by the presence of similar HSE-bearing nanominerals and nanoparticles in erupted lavas and by experimental results.

Our observations highlight that if a fraction of the HSE is incorporated into the melt as nanoparticles or immiscibile nanomelts by physical processes during partial melting of mantle peridotite, they could potentially represent a significant repository for HSE in the silicate melts. Thus, mantle melts *en route* toward the crust may transport these sulfide droplets and their cargo of HSE-nanoparticles (HSE-NPs) or nanomelts (HSE-NMs), exerting a yet unforeseen control on the ore potential of primitive metal-rich magmas as in the following cases:

5.1. Magmatic Ni-Cu-(PGE) and PGE (sulfide) deposits

These types of deposits are genetically linked to mantle melts that accessed the crust through trans-lithospheric discontinuities in tectonically active craton margins. Clusters of HSE-NPs and/or HSE-NMs (and other chalcophile and siderophile elements) might be efficiently partitioned into solid or liquids from these mantle melts to be later concentrated in-situ to form the PGE ores (Helmy et al., 2013; Tredoux et al., 1995). Efficient transport of the HSE as isolated nano-scale material would require a relatively fast ascent, which is favored when interconnected magmatic pathways exist between the SCLM and overlying

crust (Holwell et al., 2019; McDonald et al., 1995). In a later stage, the magmas carrying these sulfide melts hosting HSE-NPs or HSE-NMs may be contaminated with crustal material. Some of these "old" HSE-NPs may be preserved in melts while others may combine with semimetals in the zones with higher crustal assimilation allowing the formation of a new suite of HSE-NPs and PGM at crustal conditions. In fact, Pt-rich nanoparticles with identical chemical composition were reported from the Platreef (Junge et al., 2015) and the underlying SCLM (Bultfontain mantle xenoliths; Wainwright et al., 2016). Hart and Kinloch (1989) reported erlichmanite (OsS_2) grains with mantle-like Os isotopic composition from the Merensky reef, which significantly differs from the dominant radiogenic signature seen other laurites from this mineralized reef. The preservation of these mantle mantle-like Os signature in erlichmanite can be only explained if these PGM grains crystallized from mantle-derived melts along mantle-to-crust feeder pathways or alternatively if HSE were efficiently transferred from the mantle to the crust as HSE-NPs as those suggested by Tredoux et al. (1995) and identified by means of LA-ICP-MS by Ballhaus and Sylvester (2000). Under this new perspective, high tenors in sulfide and/or chromite-rich horizons could then be attributed to the effects of a "second" PGE enrichment considering the role that sulfide and/or oxides like chromite may play as physical collectors of these mineral particles in the crustal magmatic chamber. The implications of our model extend to the transport and deposition of Ni-, Cu- and PGE sulfides in magmatic ore deposits, where it is clearly not safe to assume that sulfide melt always tends to be dissolved upon the quick ascent of the komatiitic magma. This is clearly a fertile field for further investigation.

5.2. Au-rich deposits

The identification of gold minerals in metasomatic silicate glasses and minerals in xenoliths that have sampled the SCLM underlying auriferous continental crusts in Patagonia, Mexico, Spain, Spitsbergen, and Kaapvaal links the fertility of the magmas to the extraction and transport of gold as nanoparticles. This has been proposed as a key ingredient in the production of parental magmas responsible for the formation of magmatic-hydrothermal deposits and districts in auriferous crust from Patagonia, Spitsbergen, and Kaapvaal (e.g., Saunders et al., 2018; Tassara et al., 2017). The new observations on the presence of several nano-to-micron size particles of gold in pentlandite blebs hosted in metasomatic pyroxene of Tallante in southern Spain are also consistent with previous observations from the lamprophyre dykes of El Tale (Fortuna, Province of Murcia). The latter rocks, which originated from mantle-derived melts, also contain particles of up to 5 μm across of native gold derived from a subduction-metasomatized SCLM (Toscani, 1999). Both xenoliths and lamprophyre dykes are related to the magmatism that formed Au—Ag epithermal deposits (Carrillo-Rósua et al., 2002). The existence of nanoparticles of gold in partly altered pentlandite blebs hosted in the interstitial glass from La Breña mantle xenoliths could also be linked with a gold-metasomatized mantle. This mantle also underlies a crust with remarkable areal concentration of silver and gold deposits along the San-Luis-Tepehuanes fault system, such as the Ag—Au epithermal deposits of the Concreto de Comonfort, San Lucas de Ocampo and Avino mining districts (Camprubí, 2009).

Supplementary data to this article can be found online at https://doi.org/10.1016/j.lithos.2020.105681.

Declaration of Competing Interest

The authors declare that they have no known competing financial interests or personal relationships that could have appeared to influence the work reported in this paper.

Acknowledgements

We thank Laurie Reisberg, Hannah Hughes and an anonymous referee for their criticism, which greatly improved the quality of our manuscript. We also are indebted to Prof. Sisir K. Mondal for Editorial handling of this work and their constructive edits. This research was supported by Spanish projects: RTI2018-099157-A-I00, CGL2015-65824-P and CGL2016-81085-R granted by the "Ministerio de Ciencia, Innovación y Universidades" and Ministerio de Economía y Competitividad" (MINECO), respectively. Additional funding was provided by the Ramón y Cajal Fellowship RYC-2015-17596 and Junta de Andalucía project B-RNM-189-UGR18 to JMGJ, and the BES-2017-079949 fellowship to ES. This work was also supported by the Mexican research programs CONACYT-Ciencia Básica (A1-S-14574) and UNAM-PAPIIT grant IA-101419 awarded to VC. A. Jiménez-Franco also acknowledge a postdoctoral grant (CVU 350809) from the National Council on Science and Technology (CONACYT) of Mexico. Research grants, infrastructures and human resources leading to this research have benefited from funding by the European Social Fund and the European Regional Development Fund. We are grateful to Prof. José Jorge Aranda Gómez who provided the xenolith samples of La Breña (Durango Volcanic Field, Central Mexico). María del Mar Abad, Isabel Sánchez Almazo and Rocío Márquez Crespo (CIC, University of Granada) are acknowledged for her assistance with HRTEM, and HR-SEM and FE-SEM analysis, respectively. We are also indebted to Miguel Ángel Hidalgo Laguna from CIC of University of Granada and Xavier Llovet from the *Centres Científics i Tecnològics of the Universitat of Barcelona (CCiTUB)* for their careful help with EMPA.

References

Alard, O., Griffin, W.L., Pearson, N.J., O'Reilly, S.Y., 2002. New insights into the Re-Os systematics of sub-continental lithospheric mantle from in situ analysis of sulphides. Earth Planet. Sci. Lett. 203, 651–663.

Alard, O., Lorand, J.P., Reisberg, L., Bodinier, J.L., Dutria, J.M., O'Reilly, S.Y., 2011. Volatile-rich metasomatism in Monteferrier xenoliths (Southern France): consequence for chalcophile and highly siderophile element abundance in an orogenic-type subcontinental mantle segment. J. Petrol. https://doi.org/10.1093/petrology/egr038.

Andersen, T., Griffin, W.L., O'Reilly, S.Y., 1987. Primary sulphide melt inclusions in mantle-derived megacrysts and pyroxenites. Lithos 20, 279–294.

Andrews, D.R.A., Brenan, J.M., 2002. The solubility of ruthenium in sulfide liquid: implications for platinum group mineral stability and sulfide melt–silicate melt partitioning. Chem. Geol. 192, 163–181.

Anenburg, M., Mavrogenes, J.A., 2016. Experimental observations on noble metal nanonuggets and Fe-Ti oxides, and the transport of platinum group elements in silicate melts. Geochim Cosmochia Acta 192, 258–278.

Anenburg, M., Mavrogenes, J.A., 2020. Noble metal nanonugget insolubility in geological sulfide liquids. Geology https://doi.org/10.1130/G47579.1.

Ballhaus, C., Sylvester, P., 2000. Noble metal enrichment processes in the Merensky Reef. Bushveld Complex: J. Petrol. 41, 545–561.

Barnes, S.-J., Dare, S.A.S., 2010. Pd diffusion into pentlandite evidence from laser ablation. Goldschmidt Conference Abstract 2010, A54.

Barnes, S.-J., Cox, R.A., Zientek, M., 2006. Platinum-group element, Gold, Silver and Base Metal distribution in compositionally zoned sulfide droplets from the Medvezky Creek Mine, Noril'sk, Russia. Contrib. Mineral. Petrol. 152, 187–200.

Barnes, S.J., Pagé, P., Prichard, H.M., Zientek, M.L., Fisher, P.C., 2016. Chalcophile and platinum-group element distribution in the ultramafic series of the Stillwater complex, Mt, USA— implications for processes enriching chromite layers in Os, Ir, Ru, and Rh. Mineral. Deposita 51, 25–47.

Bishop, F.C., Smith, J.V., Dawson, J.B., 1975. Pentlandite-magnetite intergrowth in De Beers spinel lherzolite: review of sulfide nodules. Phys. Chem. Earth 9, 323–337.

Bockrath, C., Ballhaus, C., Holzheid, A., 2004a. Fractionation of the platinum-group elements during mantle melting. Science 305, 1951–1953.

Bockrath, C., Ballhaus, C., Holzheid, A., 2004b. Stabilities of laurite RuS_2 and monosulphide liquid solution at magmatic temperature. Chem. Geol. 208, 265–271.

Brenan, J.M., Andrews, D., 2001. High-temperature stability of Laurite and Ru–Os–Ir alloy and their role in PGE fractionation in mafic magmas. Can. Mineral. 39, 341–360.

Brenan, J., Bennett, N., Zajacz, Z., 2016. Experimental results on fractionation of the highly siderophile elements (HSE) at variable pressures and temperatures during planetary and magmatic differentiation. Rev. Mineral. Geochem. 81, 1–87. https://doi.org/10.2138/rmg.2016.81.1.

Camprubí, A., 2009. Major metallogenic provinces and epochs of Mexico. SGA News. 25, pp. 1–20.

Carrillo-Rósua, F.J., Morales-Ruano, S., Hach-Alí, P., 2002. The three generations of gold in the Palai-Islica epithermal deposit, southeastern Spain. Can. Mineral. 40, 1465–1481.

Ciobanu, C.L., Cook, N.J., Utsunomiya, S., Pring, A., Green, L., 2011. Focussed ion beam - transmission electron microscopy applications in ore mineralogy: bridging micron- and nanoscale observations. Ore Geol. Rev. 42, 6–31.

Delpech, G., Lorand, J.-P., Grégoire, M., Cottin, J.Y., O'Reilly, S., 2012. In-situ geochemistry of sulfides in highly metasomatized mantle xenoliths from Kerguelen, southern Indian Ocean. Lithos 154, 296–314.

Djon, M.L.N., Barnes, S.-J., 2012. Changes in sulfides and platinum-group minerals with the degree of alteration in the Roby, Twilight, and High Grade zones of the Lac des Iles complex, Ontario, Canada. Mineral. Deposita 47, 1–22.

Doyle, C.D., Naldrett, A.J., 1987. The oxygen content of "sulphide" magma and its effect on the partitioning of nickel between coexisting olivine and molten ores. Econ. Geol. 82, 208–211.

Ferraris, C., Lorand, J.P., 2015. Novodneprite ($AuPb_3$), anyuiite [$Au(Pb, Sb)_2$] and gold micro- and nano-inclusions within plastically deformed mantle-derived olivine from the Lherz peridotite (Pyrenees, France): a HRTEM–AEM–EELS study. Phys. Chem. Miner. 42, 143–150.

Fleet, M.E., Pan, Y., 1994. Fractional crystallization of anhydrous sulfide liquid in the system Fe-Ni-Cu-S, with application to magmatic sulfide deposits. Geochim. Cosmochim. Acta 58, 3369–3377.

Fleet, M.E., Stone, W.E., 1991. Partitioning of platinum-group elements in the Fe-Ni-S system and their fractionation in nature. Geochim. Cosmochim. Acta 55, 245–253.

Fleet, M.E., Chryssoulis, S.L., Stone, W.E., Weisener, C.G., 1993. Partitioning of platinum-group elements and Au in the Fe-Ni-Cu-S system: experiments on the fractional crystallization of sulfide melt. Contrib. Mineral. Petrol. 115, 36–44.

Fonseca, R.O.C., Laurenz, V., Mallmann, G., Luguet, A., Hoehne, N., Jochum, K.P., 2012. New constrains on the genesis and long-term stability of Os-rich alloys in the Earth's mantle. Geochim. Cosmochim. Acta 87, 227–242.

Fonseca, R.O.C., Brückel, K., Bragagni, A., Leitzke, F.P., Speelmanns, I.M., Wainwright, A.N., 2017. Fractionation of Rhenium from Osmium during noble metal alloy formation in association with sulfides: Implications for the interpretation of model ages in alloy-bearing magmatic rocks. Geochim. Cosmochim. Acta 216, 184–200.

Gaetani, G.A., Grove, T.L., 1999. Wetting of mantle olivine by sulfide melt: Implications for Re/Os ratios in mantle peridotite and late-stage core formation. Earth Planet. Sci. Lett. 169, 147–163.

Garuti, G., Gorgoni, C., Sighinolfi, G.P., 1984. Sulfide mineralogy and chalcophile and siderophile element in the Ivrea-Verbano mantle peridotites (Western Italian Alps). Earth Planet. Sci. Lett. 70, 69–87.

González-Jiménez, J.M., Gervilla, F., Proenza, J.A., Kerestedjian, T., Augé, T., Bailly, L., 2009. Zoning of laurite (RuS_2)-erlichmanite (OsS_2): implications for the genesis of PGM in ophiolite chromitites. Eur. J. Mineral. 21, 419–432.

González-Jiménez, J.M., Roqué-Rosell, J., Jiménez-Franco, A., Tassara, S., Nieto, F., Gervilla, F., Baurier, S., Proenza, J.A., Saunders, E., Deditius, A., Schilling, M., Corgne, A., 2019. Magmatic platinum nanoparticles in metasomatic silicate glasses and sulfides from Patagonian mantle xenoliths. Contrib. Mineral. Petrol. 174, 47.

Griffin, W.L., Spetsius, Z.V., Pearson, N.J., O'Reilly, S.Y., 2002. In situ Re-Os analysis of sulfide inclusions in kimberlitic olivine: new constraints on depletion events in the Siberian lithospheric mantle. Geochem. Geophys. Geosyst. 11, 1069.

Griffin, W.L., Graham, S., O'Reilly, S.Y., Pearson, N.J., 2004. Lithosphere evolution beneath the Kaapvaal Craton: Re–Os systematics of sulfides in mantle-derived peridotites. Chem. Geol. 208, 89–118.

Guo, J., Griffin, W.L., O'Reilly, S.Y., 1999. Geochemistry and origin of sulphide minerals in mantle xenoliths: Qiling, southeastern China. J. Petrol. 40, 1125–1149.

Gutiérrez-Narbona, R., 1999. Implicaciones metalogénicas (cromo y elementos del grupo del platino) de los magmas/fluidos residuales de un proceso de percolación a gran escala en los macizos ultramáficos de Ronda y Ojén (Béticas, Sur de España). Ph. D. Thesis. University of Granada, Spain.

Hart, S.R., Kinloch, E.D., 1989. Osmium isotope systematics in Witwatersrand and Bushveld ore deposits. Econ. Geol. 84, 1651–1655. https://doi.org/10.2113/gsecongeo.84.6.1651.

Helmy, H.M., Botcharnikov, R., 2020. Experimental determination of the phase relations of Pt and Pd antimonides and bismuthinides in the Fe-Ni-Cu sulfide systems between 1100 and 700 °C. Am. Mineral. 105, 344–352.

Helmy, H.M., Ballhaus, C., Fonseca, R.O.C., Wirth, R., Nagel, T., Tredoux, M., 2013. Noble metal nanoclusters and nanoparticles precede mineral formation in magmatic sulphide melts. Nat Commun., s3405 https://doi.org/10.1038/ncomm.

Helmy, H., Ballhaus, C., Fonseca, R., Leitzke, F., 2020. Concentrations of Pt, Pd, S, As, Se and Te in silicate melts at sulfide, arsenide, selenide and telluride saturation: evidence of PGE complexing in silicate melts? Contrib. Mineral. Petrol 175, 65. https://doi.org/10.1007/s00410-020-01705-0.

Holwell, D.A., Keays, R.R., McDonald, I., Williams, M.R., 2015. Extreme enrichment of Se, Te, PGE and Au in Cu sulfide microdroplets: evidence from LA-ICP-MS analysis of sulphides in the Skaergaard Intrusion, East Greenland. Contrib. Mineral. Petrol. 170, 53.

Holwell, D.A., Fiorentini, M., McDonald, I., Lu, Y., Giuliani, A., Smith, D.J., Keith, M., Locmelis, M., 2019. A metasomatized lithospheric mantle control on the metallogenic signature of post-subduction magmatism. Nat. Commun. 10, 3511.

Hughes, H.S.R., McDonald, I., Faithfull, J.W., Upton, B.G.J., Loocke, M., 2016. Cobalt and precious metals in sulphides of peridotite xenoliths and inferences concerning their distribution according to geodynamic environment: a case study from the Scottish lithospheric mantle. Lithos 240–243, 202–227.

Hughes, H.S.R., McDonald, I., Loocke, M., Butler, I.B., Upton, B.G.J., Faithfull, J.W., 2017. Paradoxical co-existing base metal sulphides in the mantle: the multi-event record preserved in Loch Roag peridotite xenoliths, North Atlantic Craton. Lithos 276, 103–121.

Jugo, P.J., Wilke, M., Botcharnikov, R.E., 2010. Sulfur K-edge XANES analysis of natural and synthetic basaltic glasses: implications for S speciation and S content as function of oxygen fugacity. Geochim. Cosmochim. Acta 74, 5926–5938 pp. 103-121.

Junge, M., Wirth, R., Oberthür, T., Melcher, F., Schreiber, A., 2015. Mineralogical sitting of platinum-group elements in pentlandite from the Bushveld complex, South Africa. Mineral. Deposita 50, 41–54.

Kamenetsky, V., Zelenski, M., 2020. Origin of Noble-Metal Nuggets in Sulfide-Saturated Arc Magmas: A Case Study of Olivine-Hosted Sulfide Melt Inclusions from the Tolbachik Volcano. Kamchatka, Russia.

Kamenetsky, V.S., Park, J.-W., Mungall, J.E., Pushkarev, E.V., Ivanov, A.V., Kamenetsky, M.B., Yaxley, G.M., 2015. Crystallization of platinum-group minerals from silicate melts: evidence from Cr-spinel–hosted inclusions in volcanic rocks. Geology 43, 903–906.

Karup-Møller, S., Makovicky, E., 1993. The system Pd-Ni-S at 900°, 725°, 550° and 400°. Econ. Geol. 88, 1261–1268.

Keays, R.R., Sewell, D.K.B., Mitchell, R.H., 1981. Platinum and palladium minerals in upper mantle-derived lherzolites. Nature 294, 646–648.

Kitakaze, A., Machida, T., Komatsu, R., 2016. Phase relations in the Fe-Ni-S system from 875 to 650 °C. Can. Mineral. 54, 1175–1186.

Kogiso, T., Suzuki, K., Suzuki, T., Shinotsuka, K., Uesugi, K., Takeuchi, A., Suzki, Y., 2008. Detecting micrometer-scale platinum-group minerals in mantle peridotite with microbeam synchrotron radiation X-ray fluorescence analysis. Geochem. Geophys. Geosyst. 9, Q03018. https://doi.org/10.1029/2007GC001888.

König, S., Lissner, M., Lorand, J.-P., Bragagni, A., Luguet, A., 2015. Mineralogical control of selenium, tellurium and highly siderophile elements in the Earth's mantle: evidence from mineral separates of ultra-depleted mantle residues. Chem. Geol. 396, 16–24.

Kravchenko, T.A., 2009. Pt-Pd-Sn intermetallic compounds crystallized from Cu-Fe sulfide melt. New data on Minerals 44, 66–72.

Kullerud, G., Yund, R.A., Moh, G.H., 1969. Phase relations in the Cu-Fe-S, Cu-Ni-S and Fe-Ni-S systems. In: Wilson, H.D.B. (Ed.), Magmatic Ore Deposits. Economic Geology Publishing Co., Lancaster, Pennsylvania, pp. 323–343.

Larocque, A., Stimac, J., Keith, J., Huminicki, M., 2000. Evidence for open-system behavior in immiscible Fe-S-O liquids in silicate magmas: implications for contributions of metals and sulfur to ore-forming fluids. Can. Mineral. 38, 1233–1249.

Lee, M., 2010. Transmission electron microscopy (TEM) of earth and planetary materials: a review. Mineral. Mag. 74, 1–27.

Li, Y., Audétat, A., 2013. Gold solubility and partitioning between sulfide liquid, monosulfide solid solution and hydrous mantle melts: implications for the formation of Au-rich magmas and crust-mantle differentiation. Geochim. Cosmochim. Acta 118, 247–262.

Li, C., Barnes, S.-J., Makovicky, E., Rose-Hansen, J., Makovicky, M., 1996. Partitioning of nickel, copper, iridium, rhodium platinum and palladium between monosulphide solid solution and sulphide liquid: effects of composition and temperature. Geochim. Cosmochim. Acta 60, 1231–1238.

Li, Y., Feng, L., Kiseeva, E.S., Gao, Z., Guo, H., Du, Z., Wang, F., Shi, L., 2019. An essential role for sulfur in sulfide-silicate melt partitioning of gold and magmatic gold transport at subduction settings. Earth Planet. Sci. Lett. 528, 115850.

Lorand, J.P., Alard, O., Luguet, A., 2010. Platinum-group element micronuggets and refertilization process in Lherz orogenic peridotite (northeastern Pyrenees, France). Earth Planet. Sci. Lett. 289, 298–310.

Luguet, A., Reisberg, L., 2016. Highly Siderophile Element and ^{187}Os Signatures in Non-cratonic Basalt-hosted Peridotite Xenoliths: Unravelling the Origin and Evolution of the Post-Archean Lithospheric Mantle. Rev. Mineral. Geochem. 81, 305–367.

Luguet, A., Shirey, S.B., Lorand, J.P., Horan, M.F., Carlson, R.W., 2007. Residual platinum-group minerals from highly depleted harzburgites of the Lherz massif (France) and their role in HSE fractionation of the mantle. Geochim. Cosmochim. Acta 71, 3082–3097.

Majzlan, J., Makovicky, M., Makovicky, E., Rose-Hansen, J., 2002. The system Fe–Pt–S at 1100°C. Can. Mineral. 40, 509–517.

Makovicky, E., 2002. Ternary and quaternary phase systems with PGE. In: Cabri, L.J. (Ed.), The Geology, Geochemistry, Mineralogy and Mineral Beneficiation of Platinum-Group Elements. Canadian Institution of Mining Metallurgy and Petroleum, Montreal, pp. 131–178.

Makovicky, E., Karup-Møller, S., 1993. The system Pd-Fe-S at 900°, 725°, 550° and 400°. Econ. Geol. 88, 1269–1278.

Makovicky, M., Makovicky, E., Rose-Hansen, J., 1986. Experimental studies on the solubility and distribution of platinum group elements in base metal sulphides in platinum deposits. In: Gallagher, M.J., Lxer, R.A., Neary, C.R., Priehard, H.M. (Eds.), Metallurgy of basic and ultrabasic rocks. The Institution of Mining and Metallurgy, London, pp. 415–425.

Makovicky, M., Makovicky, E., Rose-Hansen, J., 1988. Experimental evidence of the formation and mineralogy of platinum and palladium ore deposits. In: Boissonnas, J., Omenetto, P. (Eds.), Mineral Deposits within the European Community. Berlin- Heidelberg, Springer-Verlag, pp. 303–317.

Makovicky, E., Karup-Mcfller, S., Makovicky, M., Rose-Hansen, J., 1990. Experimental studies on the phase systems Fe-Ni-Pd-S and Fe-Pt-Pd-As-S applied to PGE deposits. Mineral. Petrol. 42, 307–313.

Mann, U., Frost, D., Rubie, D., Becker, H., Audetat, A., 2012. Partitioning of Ru, Rh, Pd, Re, Ir and Pt between liquid metal and silicate at high pressures and high temperatures - Implications for the origin of highly siderophile element concentrations in the Earth's mantle. Geochim. Cosmochim. Acta 84, 593–613. https://doi.org/10.1016/j.gca.2012.01.026.

Mavrogenes, J.A., O'Neill, H.S.C., 1999. The relative effects of pressure, temperature and oxygen fugacity on the solubility of sulfide in mafic magmas. Geochemica et Cosmochimica Acta 63, 1173–1180.

McDonald, I., de Wit, M.J., Smith, C.D., Bizzi, L.A., Viljoen, K.S., 1995. The geochemistry of the platinum-group elements in Brazilian and southern African kimberlites. Geochim. Cosmochim. Acta 59, 2883–2903.

Médard, E., Schmidt, M.W., Wälle, M., Keller, N.S., Günther, D., 2015. Platinum partitioning between metal and silicate melts: Core formation, late veneer and the nanonuggets issue. Geochim. Cosmochim. Acta 162, 183–201.

Melekhova, E., Blundy, J., Martin, R., Arculus, R., Pichavant, M., 2017. Petrological and experimental evidence for differentiation of water-rich magmas beneath St. Kitts, Lesser Antilles. Contributions to Mineral and. Petrology 172, 98. https://doi.org/10.1007/s00410-017-1416-3.

Mundl, A., Ntaflos, T., Ackerman, L., Bizimis, M., Bjerg, E.A., Wegner, W., Hauzenberger, C.A., 2015. Geochemical and Os-Hf-Nd-Sr Isotopic Characterization of North Patagonian Mantle Xenolith: Implications for Extensive Melt Extraction and Percolation.

Mungall, J.E., Brenan, J.M., 2014. Partitioning of platinum-group elements and au between sulfide liquid and basalt and the origins of mantle-crust fractionation of the chalcophile elements. Geochim. Cosmochim. Acta 125, 265–289.

Mungall, J.E., Andrews, D.R.A., Cabri, L.J., Sylvester, P.J., Tubrett, M., 2005. Partitioning of Cu, Ni, Au, and platinum-group elements between monosulfide solid solution and sulfide melt under controlled oxygen and sulfur fugacities. Geochim. Cosmochim. Acta 69, 4349–4360.

Naldrett, A.J., 1969. A portion of the system Fe—S—O between 900 and 1080°C and its application to sulfide ore magmas. J. Petrol. 10, 171–201.

O'Driscoll, B., González-Jiménez, J.M., 2016. Petrogenesis of the Platinum-Group Minerals. Rev. Mineral. Geochem. 81, 489–578.

Peregoedova, A.V., 1998. The experimental study of the Pt-Pd-partitioning behaviour between monosulfide solid solution and Cu-Ni-sulfide melt at 900–840 °C 8th International Platinum Symposium Abstracts: Geological Society South Africa and South African Institute of Mining and Metallurgy Symposium Series. S18 pp. 325–327.

Peregoedova, A.V., Ohnenstetter, M., 2002. Collectors of Pt, Pd and Rh in a S-poor Fe–Ni–Cu–sulfide system at 760 °C: experimental data and application to ore deposits. Can. Mineral. 40, 527–561.

Peregoedova, A., Barnes, S.J., Baker, D.R., 2004. The formation of Pt–Ir alloys and Cu–Pd-rich sulfide melts by partial desulfurization of Fe–Ni–Cu sulfides: results of experiments and implications for natural systems. Chem. Geol. 208, 247–264.

Piña, R., Gervilla, F., Barnes, S.J., Ortega, L., Lunar, R., 2012. Distribution of platinum-group and chalcophile elements in the Aguablanca Ni–Cu sulfide deposit (SW Spain): evidence from a LA-ICP-MS study. Chem. Geol. 302–303, 61–75.

Pruseth, K.L., Palme, H., 2004. The solubility of Pt in liquid Fe-sulfides. Chem. Geol. 208, 223–245.

Robertson, J.C., Barnes, S.J., Le Vaillant, M., 2016. Dynamics of magmatic sulphide droplets during transport in silicate melts and implications for magmatic sulphide ore formation. J. Petrol. 56, 2445–2472.

Saunders, J.E., Pearson, N.J., O'Reilly, S.Y., Griffin, W.L., 2015. Sulphide metasomatism and the mobility of gold in the lithospheric mantle. Chem. Geol. 410, 149–161.

Saunders, J.E., Pearson, N.J., O'Reilly, S.Y., Griffin, W.L., 2018. Gold in the mantle: a global assessment of abundance and redistribution processes. Lithos 322, 376–391.

Shelton, K.L., Merewether, P.A., Skinner, B.J., 1981. Phases and phase relations in the system Pd-Pt-Sn. Can. Mineral. 19, 599–605.

Shinshin, D., Jak, E., Decterov, S.A., 2015. Critical assessment and thermodynamic modeling of the Fe-O-S system. J. Phase Equilib. Diffus. 36, 224–240.

Sinyakova, E., Kosyakov, V., Distler, V., Karmanov, N., 2016. Behaviour of Pt, Pd, and au during crystallization of Cu-rich magmatic sulfide minerals. Can. Mineral. 45, 491–509.

Sinyakova, E., Kosyakov, V., Palyanova, G., Karmanov, N., 2019. Experimental modeling of noble and chalcophile element fractionation during solidification of Cu-Fe-Ni-S melt. Minerals 9, 531. https://doi.org/10.3390/min9090531.

Sisson, T.W., 2003. Native gold in Hawaiian alkali magma. Econ. Geol. 98, 643–648.

Sugaki, A., Kitakaze, A., 1998. High form of pentlandite and its thermal stability. Am. Mineral. 83, 133–140.

Szabó, Cs, Bodnar, R.J., 1995. Chemistry and origin of mantle sulfides in spinel peridotite xenoliths from alkaline basaltic lavas, Nógrád-Gömör Volcanic Field, northen Hungary and southern Slovakia. Geochim. Cosmochim. Acta 59, 3917–3927.

Tassara, S., González-Jiménez, J.M., Reich, M., Schilling, M.E., Morata, D., Begg, G., Saunders, E., Griffin, W.L., O'Reilly, S.Y., Grégoire, M., Barra, F., Corgne, A., 2017. Plume-subduction interaction forms large auriferous provinces. Nat. Commun. 8, 843.

Tassara, S., González-Jiménez, J.M., Reich, M., Saunders, E., Luguet, A., Morata, D., Grégoire, M., van Acken, D., Schilling, M.E., Barra, F., Nowell, G., Corgne, A., 2018. Highly siderophile elements mobility in the subcontinental lithospheric mantle beneath southern Patagonia. Lithos 314–315, 579–596.

Tassara, S., Reich, M., Konecke, B.A., González-Jiménez, J.M., Simon, A.c., Morata, D., Barra, F., Fiege, A., Schilling, M.E., Corgne, A., 2020. Unraveling the effects of melt-mantle interactions on the gold fertility of magmas. Front. Earth Sci. 11. https://doi.org/10.3389/feart.2020.00029.

Toscani, L., 1999. Magmatic gold grains in the El Tale lamproite, Fortuna, SE Spain. Mineral. Mag. 63, 595–602.

Tredoux, M., Lindsay, N.M., Davies, G., McDonald, L., 1995. The fractionation of platinum-group elements in magmatic systems, with the suggestion of a novel causal mechanism. S. Afr. J. Geol. 98, 157–167.

Wainwright, A.N., Luguet, A., Schreiber, A., Fonseca, R.O.C., Nowell, G.M., Lorand, J.-P., Wirth, R., Janney, P.E., 2016. Nanoscale variations in ^{187}Os isotopic composition and HSE systematics in a Bultfontein peridotite. Earth Planet. Sci. Lett. 447, 60–71.

Wang, K.L., O'Reilly, S.Y., Griffin, W.L., Pearson, N.J., Zhang, M., 2009. Sulfides in mantle peridotites from Penghu Island, Taiwan: melt percolation, PGE fractionation, and the lithospheric evolution of the South China block. Geochim. Cosmochim. Acta 73, 4531–4557.

Wirth, R., 2004. Focused Ion Beam (FIB): a novel technology for advanced application of micro- and nanoanalysis in geosciences and applied mineralogy. Eur. J. Mineral. 16, 863–876.

Wirth, R., 2009. Focused Ion Beam (FIB) combined with SEM and TEM: advanced analytical tools for studies of chemical composition, microstructure and crystal structure in geomaterials on a nanometre scale. Chem. Geol. 261, 217–229.

Wirth, R., Reid, D., Schreiber, A., 2013. Nanometer-sized platinum-group minerals (PGM) in base metal sulfides: new evidence for an orthomagmatic origin of the Merensky reef PGE ore deposit. Bushveld Complex. South Africa. Can. Mineral. 51, 143–155.

Zelenski, M., Kamenetsky, V.S., Mavrogenes, J.A., Gurenko, A.A., Danyushevsky, L.V., 2018. Silicate-sulfide liquid immiscibility in modern arc basalt (Tolbachik volcano, Kamchatka): part I. Occurrence and compositions of sulfide melts. Chem. Geol. 478, 102–111. https://doi.org/10.1016/j.chemgeo.2017.09.013.

Zelenski, M., Kamenetsky, V.S., Navrogenes, J.A., Danyushevsky, L.V., Matveev, D., Gurenko, A.A., 2017. Platinum-group elements and gold in sulfide melts from modern arc basalt (Tolbachik volcano, Kamchatka). Lithos 290-291, 172–188.

Zhang, Z., Mao, J., Wang, F., Pirajno, F., 2006. Native gold and native copper grains enclosed by olivine phenocrysts in a picrite lava of the Emeishan large igneous province, SW China. Am. Mineral. 91, 1178–1183.